iScience

Article

HIV-1 Tat protein alters medial prefrontal cortex neuronal activity and recognition memory

Graphical abstract

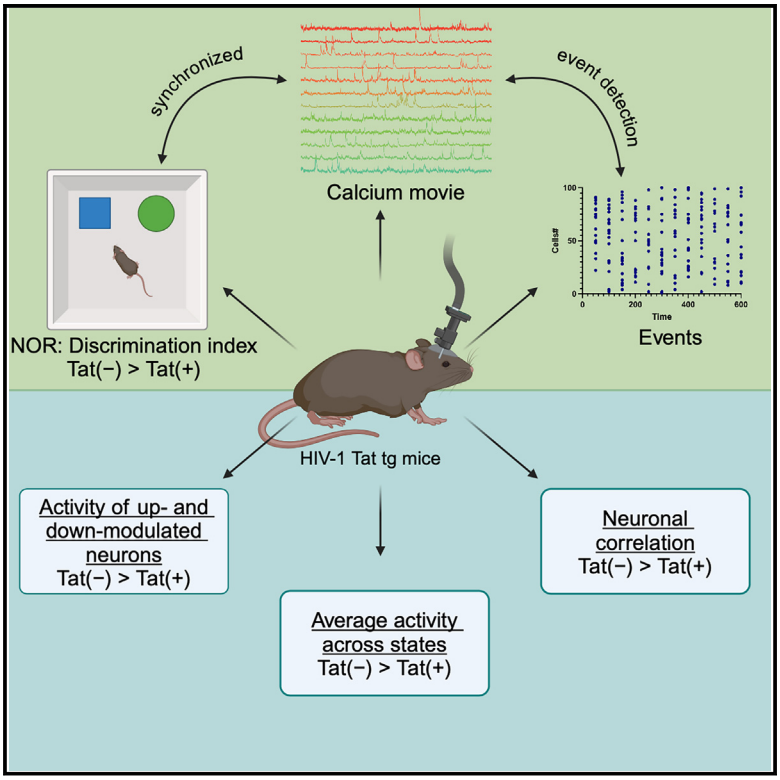

Highlights

- Single-cell imaging study in a neuroHIV Tat transgenic mouse model
- Tat expression decreases mPFC neuronal activity and hinders recognition memory
- Tat expression does not alter the number of cells that are activated in the mPFC
- Object familiarity leads to an increase in mPFC neuronal activity

Authors

Barkha J. Yadav-Samudrala, Aryan P. Yadav, Rahul P. Patel, Sylvia Fitting

Correspondence

sfitting@email.unc.edu (S.F.), barkhaj@email.unc.edu (B.J.Y.-S.)

In brief

Molecular biology; Neuroscience; Cell

Yadav-Samudrala et al., 2025, iScience *28*, 112075
March 21, 2025
https://doi.org/10.1016/j.isci.2025.112075

CellPress

iScience

CellPress
OPEN ACCESS

Article

HIV-1 Tat protein alters medial prefrontal cortex neuronal activity and recognition memory

Barkha J. Yadav-Samudrala,[1,*] Aryan P. Yadav,[2] Rahul P. Patel,[3] and Sylvia Fitting[1,4,*]
[1]Department of Psychology and Neuroscience, The University of North Carolina at Chapel Hill, Chapel Hill, NC 27599, USA
[2]Department of Computer Science, The University of North Carolina at Greensboro, Greensboro, NC 27412, USA
[3]UNC Neuroscience Center, The University of North Carolina at Chapel Hill, Chapel Hill, NC 27599, USA
[4]Lead contact
*Correspondence: sfitting@email.unc.edu (S.F.), barkhaj@email.unc.edu (B.J.Y.-S.)
https://doi.org/10.1016/j.isci.2025.112075

SUMMARY

Despite advancements in combined antiretroviral therapy, human immunodeficiency virus (HIV)-associated neurocognitive disorder (HAND) continue to affect 40%–50% of people living with HIV. While neuroimaging studies have revealed HIV-1-induced alterations in cortical networks and brain macrostructures, it still remains unclear how individual neurons in the medial prefrontal cortex (mPFC) are affected during recognition memory. Using *in vivo* calcium imaging in an HIV-1 transactivator of transcription (Tat) transgenic mouse model, we examined mPFC neuronal activity during a novel object recognition memory task. Our findings show that HIV Tat expression reduces overall neuronal activity in Tat(+) mice without altering the number of activated cells. Moreover, distinct neuronal subpopulations are up- and downmodulated in both Tat(−) and Tat(+) mice depending on object exploration. Importantly, familiarity-driven increases in mPFC activity were disrupted by HIV Tat expression. These findings enhance our understanding of HAND and may inform future pharmacological strategies aimed at restoring cognitive function.

INTRODUCTION

For the past four decades, the human immunodeficiency virus type 1 (HIV-1) has infected approximately 84 million people worldwide and has cost the lives of over 40 million people,[1] with no cure currently in sight. Over the years, the development of combined antiretroviral therapy (cART) has had a profound impact on the management of the infection, leading to the number of people living with HIV-1 (PLWH) steadily increasing.[1] However, evidence suggests that despite the effectiveness of cART, the HIV-1 virus enters the central nervous system (CNS) early in infection through the blood brain barrier (BBB) via infected macrophages, monocytes, T cells, and directly as cell-free virus.[2–6] After crossing the BBB, the cell-free virus establishes CNS reservoirs by infecting brain endothelial cells, microglia and astrocytes, but not neurons.[7–10] The currently approved cART drugs do not cross the BBB effectively,[11] making it difficult to target the virus within the CNS; thus, leading to the development of HIV-associated neurocognitive disorder (HAND). Approximately 40%–50% of PLWH are estimated to exhibit HAND symptoms; therefore, it remains a global concern.[12,13] Managing symptoms of HAND is difficult, especially during the cART era, as heterogeneity of cognitive deficits exists between individuals and is further altered with disease progression.[14] Neurocognitive deficits associated with HAND include specifically learning and memory,[15–21] but also attention and working memory, executive function, motor coordination, and sensory perception.

HIV-1 infection contributes to HAND in cART-controlled PLWH through the continued production and release of neurotoxic HIV-1 proteins, such as transactivator of transcription (Tat), from cellular reservoirs within the CNS.[22] Tat is the first viral protein produced upon infection of a cell[23] and drives viral synthesis by regulating proviral genome transcription.[24,25] It is known that Tat can exert its effects on neurons directly by interacting with the *N*-methyl-*D*-aspartate receptors (NMDARs) and depolarizing the neurons to facilitate its neurotoxicity.[26–28] Tat is also known to sequester zinc and disrupt zinc-mediated regulation of NMDAR.[29] Indirectly, Tat affects the intermediary function of non-neuronal cells, such as microglia and/or astrocytes.[30] The release of Tat from infected cells can activate infected non-neuronal cells as well as bystander glial cells to promote inflammatory response,[31,32] which can lead to neuronal damage, including dendritic simplification, axonal disruption, and synaptic loss.[16,24,33] Additionally, Tat exposure also causes an increase in intracellular calcium, triggering apoptosis through the endoplasmic reticulum,[34,35] triggering reactive oxygen species (ROS) production,[36] and dysregulating the expression of synaptic plasticity genes.[37] Regardless by which pathway the majority of Tat effects are exerted, it ultimately leads to functional deficits in neurons.[38–40]

Numerous brain imaging studies have provided a window to explore brain structure and function in PLWH. Early studies using magnetic resonance imaging (MRI) and proton magnetic resonance spectroscopy (MRS) revealed damage within the gray and white brain matter and worse neuronal integrity in the basal ganglia and frontal regions.[41,42] Interestingly, it was revealed

that even with cART, neuronal loss and neuroinflammation persists.[43–46] Functional MRI (fMRI) studies show disruption of the frontostriatal network, which includes the striatum, anterior cingulate cortex, and frontal cortex,[44,47,48] reflecting alterations in areas responsible for cognitive performance.[49] Despite remarkable progress in understanding how HIV-1 proteins alter behavior and impact the pathophysiology within the CNS, the cellular, molecular, and mechanistic circuit interaction between HIV-1 proteins remain to be understood to gain insight into novel prevention and treatment strategies. Therefore, to understand the specific aspects of Tat underlying pathophysiology of HAND we utilized a HIV-1 Tat transgenic mouse model in this study. In this mouse model, Tat is expressed in a doxycycline inducible manner that is delivered via a specially formulated chow.[50,51] The HIV-1 Tat transgenic mouse model is a well-established model for neuroHIV as it mirrors the pathologies that are observed with HAND in the cART era,[50–53] including reduced neuronal spine density and changes in synaptic proteins[51,53,54] With regards to behavioral abnormalities, Tat transgenic mice show deficits in and learning and memory,[52,54] attentional processing,[32] motor behaviors,[55,56] anxiety- and depression-like behaviors,[55–59] all of which have been observed in PLWH with HAND. Studies demonstrating long-lasting deficiencies in the novel object recognition (NOR) task suggest that Tat exposure progressively mediates deficits.[54,60–62]

Past electrophysiological and behavioral evidence have shown that medial prefrontal cortex (mPFC) neurons carry information regarding recognition and recency discrimination,[63] which is disrupted when this region is damaged.[64–67] Various neurodegenerative diseases, such as Alzheimer's disease,[68] Huntington's disease,[69] and Parkinson's disease,[70] show PFC dysfunction. Preclinical mouse models of Alzheimer's disease display changes in PFC synaptic makers[71,72] and altered neuromodulation of synaptic transmission,[73–75] in addition to deficits in working memory, which is correlated with the accumulation of amyloid beta in the PFC.[76,77] Studies also show significant impairments in the functional connectivity between anterior cingulate and the lateral PFC, represented by the loss of neuronal synchrony between both brain structures in individuals with Huntington's disease.[69,78] Moreover, Parkinson's disease shows PFC-related working memory deficits[79] and impaired PFC dopamine signaling.[80,81] Similar to the aforementioned neurodegenerative diseases, deficits in the PFC interfering with learning and memory have also been reported in PLWH with HAND.[82] However, it is unknown how PFC neurons and their firing patterns are affected at the cellular level by Tat expression during NOR task.

In the present study we applied an *in vivo* calcium imaging approach to identify how the population activity of mPFC neurons is altered in HIV-1 Tat transgenic mice while performing the NOR task. In addition to Tat expression impairing recognition memory, we also find that the neuronal activity is significantly altered in the presence of Tat. Neurons in control Tat(−) mice are highly correlated and have overall higher neuronal activity as compared to transgenic Tat(+) mice. Further, in Tat(−) mice, the neurons show higher synchrony and activity when exploring the familiar object compared to the novel object, which is not seen for Tat(+) mice. To our knowledge, these results provide evidence that the presence of the HIV-1 Tat protein hampers the ability of mPFC neurons to discriminate between familiar and novel objects.

RESULTS

Experimental approach and HIV-1 Tat effects on novel object recognition task

Our goal in the present study was to characterize how object identity, familiar object, and novel object, are represented in HIV-1 Tat transgenic mice. Previous studies have shown that neurotoxic HIV-1 proteins released from the cellular reservoir within the CNS,[40,83,84] including the viral protein Tat,[85] can target neurons directly and cause neuronal damage, leading to loss in cognitive function. PFC-related cognition has been demonstrated to be specifically vulnerable in the post-cART era.[86,87] Therefore, we conducted microendoscopic imaging of calcium activity in medial PFC pyramidal neurons when mice performed the novel object recognition task and explored a novel and familiar objects over a 10 min time period. (Figure 1). Adeno-associated virus carrying a synapsin promoter (pAAV-Syn-GCaMP6f-WPRE-SV40)[88] was microinjected followed by implanting a gradient index (GRIN) lens implant in the left hemisphere of adult male HIV-1 Tat transgenic mice (Tat(−): $n = 5$ mice, 661 cells; Tat(+): $n = 3$ mice, 498 cells; Figure 1A). GCaMP expression was checked 6–8 weeks after viral injection, and after successful virus expression and our ability to continuously monitor mPFC activity, we moved ahead with the NOR task (Figure 1B).

The NOR task took place over a period of two days. To increase the power for behavioral testing, additional animals (males and females) were used (n = 12(6f)/genotype). All mice were tested separately in a sequential order. On day 1, mice were habituated to the open field chamber (without any objects) to lower anxiety and encourage exploration for day 2. Mice were allowed to freely explore the open field for a period of 5 min and then returned to their respective cages and brought back to the vivarium until the next day. On day 2, all the steps from day 1 were repeated but two identical objects (familiar object) were placed at equidistant from the center in the open field and mice were allowed to explore the objects for 10 min. After 1 h (intertrial interval) mice were placed back in the open field where one of the objects was replaced with a novel object. Calcium imaging from both training and testing phases were recorded for GCaMP injected mice. Following the behavioral experiments, mice were transcardially perfused, and their brains were harvested to verify the placement of microinjections and lens implants. Figures 2A and 2B (see Figure S1) shows the histology images from a representative Tat(−) mouse and Tat(+) mouse. Figures 2C and 2D shows the exploration of familiar and novel objects. The total exploration time (Figure 2E) for familiar and novel object did not show any significance difference between Tat(−) and Tat(+) mice. However, an independent t test showed a significant difference in the discrimination index between Tat(−) and Tat(+) mice ($t(22) = 4.18$, $p < 0.001$, Figure 2F). Note, that when considering GCaMP injected mice only, no significant difference was observed.

mPFC neurons are recruited during the NOR task and their activity reduces in the presence of the HIV-1 Tat protein

We focused on mPFC activity around the overall exploration of both, the familiar and novel objects. mPFC neurons were

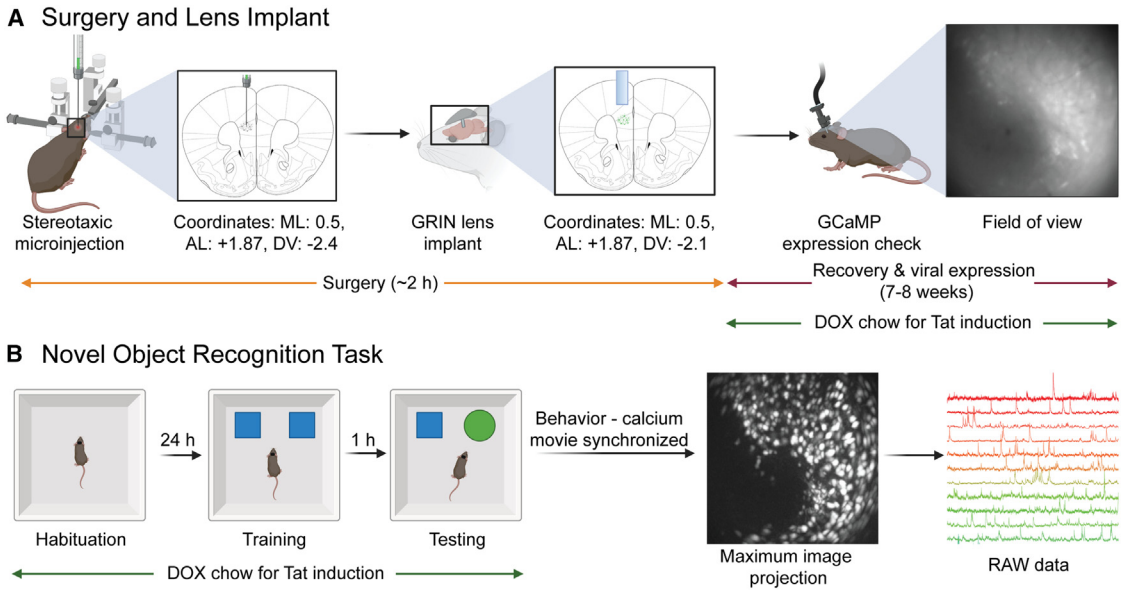

Figure 1. Experimental outline of surgery and behavioral experiments

(A) Experimental outline of stereotaxic microinjection and GRIN lens implantation and an example of field of view and GCaMP expression.

(B) Outline of novel object recognition task showing habituation, training, and testing phases. The behavioral and calcium data were synchronized and recorded at 20 frames/s. Maximum image and raw data were generated by IDPS. Created in https://BioRender.com.

recorded from the same field of view (FOV) but were not aligned across training and testing phases. The neuronal data reported in this manuscript are derived from the testing phase. Furthermore, we examined calcium signals around the period when mice actively explored one of the two objects. The individual spikes and events were generated from end-to-end CNMF-E, which was run through the IDEAS platform.

It was observed that in Tat(−) mice the neuronal activity was highly correlated when mice explored the familiar object as compared to the novel object (Figures 3A and S2 show a correlation matrix from a representative Tat(−) mouse). However, HIV-1 Tat protein expression disrupted this relationship, as Tat(+) mice demonstrated no difference in the neural activity correlation between familiar and novel objects exploration (Figures 3B and S2 show a correlation matrix from a representative Tat(+) mouse). Comparison of the cumulative distribution function of maximum cell-cell correlation between Tat(−) and Tat(+) mice revealed a significant genotype effect in familiar object exploration only (Figure 3C; Kolmogorov-Smirnov test: main genotype effect for familiar object, $D(1159) = 0.263$, $p < 0.0001$) but not for novel object exploration (Figure 3D), suggesting that during familiar object exploration the likelihood of finding correlated cell in Tat(−) mice is higher than in Tat(+) mice.

Additionally, a mean pairwise Pearson correlation of cells between familiar and novel objects exploration exhibited a strong positive correlation in Tat(−) mice (Figure 3E; Pearson correlation: $r = 0.51$, $p < 0.0001$), indicating that cells that show higher co-activation for the familiar object also show higher co-activation for the novel object. Interestingly, this synchronized activity noted for Tat(−) mice can explain 26% of the total variance in the data. In contrast, Tat(+) mice only demonstrated a weak correlation (Figure 3F; Pearson correlation: $r = 0.12$, $p = 0.005$), suggesting fewer synchronized activity between cells that only account for 1.5% of total variance.

When assessing the effect size difference between genotypes (Figure 3G), both familiar object ($t(1157) = 24.27$, $p < 0.001$) and novel object ($t(1157) = 10.47$, $p < 0.001$), showed a significant effect; however, the effect size difference when comparing Tat(−) vs. Tat(+) mice was large for familiar object exploration (Cohen's $d = 1.44$) whereas novel object exploration showed a medium effect size (Cohen's $d = 0.62$), suggesting higher differences in cell-cell correlation between genotype when exploring the familiar object as compared to the novel object. Importantly, when assessing the mean activity of cells during familiar and novel objects exploration, a two-way ANOVA demonstrated a genotype × object interaction ($F(1, 6) = 6.54$, $p = 0.04$, Figure 3H). A pairwise comparison between familiar and novel objects exploration showed a significant difference in the activity of cells in Tat(−) mice ($t(5) = 3.097$, $p = 0.03$), with mean cell activity being significantly higher during familiar object exploration as compared to novel object exploration. Whereas in Tat(+) mice the activity of cells stayed the same regardless of which object was explored.

Neuronal activity in Tat(+) mice during all four epochs is reduced compared to Tat(−) mice in both familiar and novel objects exploration

During the behavioral study, the duration and number of times mice explore familiar and novel objects varies; therefore, we analyzed the calcium activity using epochs relative to object exploration: *before*, *start*, *end*, *after*. Where *before* represents 2 s before the event, *start* and *end* are the time points mice start and end exploring either familiar or novel objects, respectively, and *after* is the calcium activity 2 s after object exploration. Figures 4A–4D (see Figure S3) shows the calcium transients

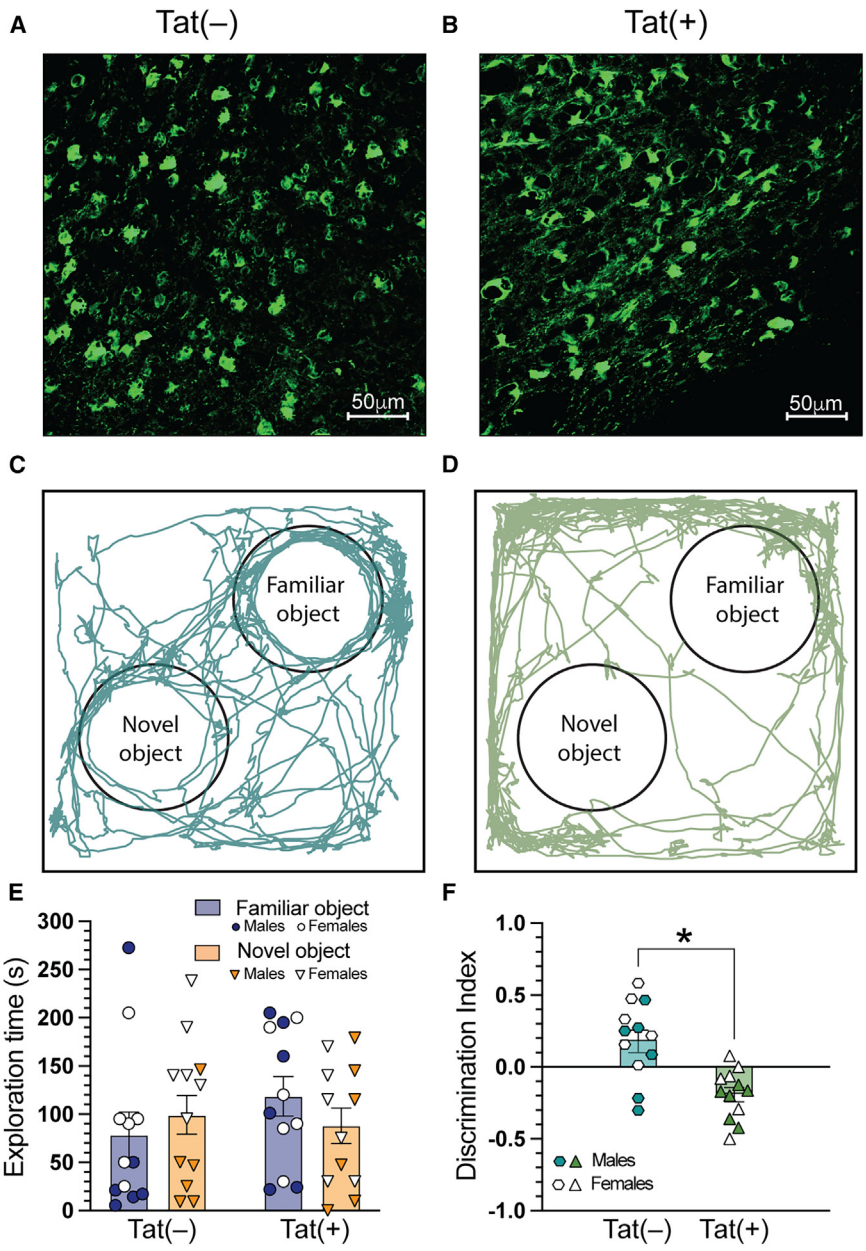

Figure 2. Experimental approach and HIV-1 Tat effects on NO recognition task

(A and B) Histology images confirming the GCaMP location in the mPFC from Tat(–) and Tat(+) mice, respectively. Scale: 50 μm

(C and D) Traces of Tat(–) and Tat(+) animals generated by Anymaze, exploring the open field arena and the objects during the testing phase of the NOR task.

(E) Quantification of total exploration time for familiar and novel objects by Tat(–) and Tat(+) mice. Two-way ANOVA: N.S. $p > 0.05$. $n = 12(6f)$/genotype.

(F) Discrimination index for Tat(–) and Tat(+) mice did not show any preference for objects. Independent t test: $^*p < 0.001$. $n = 12(6f)$/genotype. N.S., not significant.

represented as ΔF/F and Figures 4E–4H shows heatmaps from the four epochs in Tat(–) and Tat(+) mice during familiar and novel objects exploration.

The cumulative distribution function of the *Z* scores showed significant genotype differences for all four epochs for familiar and novel objects, (Figure 4I; Kolmogorov-Smirnov test: main genotype effect for *before* familiar object, $D(1202) = 0.279$, $p < 0.0001$, Figure 4I; Kolmogorov-Smirnov test: main genotype effect for *before* novel object, $D(1202) = 0.141$, $p < 0.0001$, Figure 4J; Kolmogorov-Smirnov test: main genotype effect for *start* familiar object, $D(1202) = 0.301$, $p < 0.0001$, Figure 4J; Kolmogorov-Smirnov test: main genotype effect for *start* novel object, $D(1202) = 0.116$, $p = 0.0006$, Figure 4K; Kolmogorov-Smirnov test: main genotype effect for *end* familiar object, $D(1202) = 0.294$, $p < 0.0001$, Figure 4K; Kolmogorov-Smirnov test: main genotype effect for *end* novel object, $D(1202) = 0.114$, $p = 0.0007$, Figure 4L; Kolmogorov-Smirnov test: main genotype effect for *after* familiar object, $D(1202) = 0.158$, $p < 0.0001$, Figure 4L; Kolmogorov-Smirnov test: main genotype effect for *after* novel object, $D(1202) = 0.258$, $p < 0.0001$), suggesting overall the cumulative *Z* scores for Tat(–) mice were higher as compared to Tat(+) mice for both familiar and novel objects exploration.

As expected, an independent t test revealed that the average scores overall were found to be higher in Tat(–) mice compared to Tat(+) mice for all four epochs (Figures 4M and 4N; *before* $t(2316) = 401.47$, $p = 0.004$, *start* $t(2316) = 422.98$, $p = 0.008$, *end* $t(2316) = 445.03$, $p < 0.001$, *after* $t(2316) = 428.47$, $p = 0.002$). When the average *Z* scores were compared based on the type of object being explored, Tat(–) mice had higher average *Z* score compared to Tat(+) mice based on epochs. For familiar object, except for the *before* epoch the average *Z* scores for Tat(–) mice were higher compared to Tat(+) mice (Figure 4M; *start* $t(1157) = 246.31$, $p = 0.046$, *end* $t(1157) = 299.48$, $p = 0.017$, *after* $t(1157) = 428.47$, $p = 0.015$). For novel object, significant differences between the Tat(–) and Tat(+) mice were only observed for *before* and *end* epochs (Figure 4N; *before* $t(1157) = 163.37$, $p = 0.020$, *end* $t(1157) = 168.87$, $p = 0.018$). The aforementioned data suggest that the overall activity of Tat(–) mice increases with epochs as compared to Tat(+) mice only when mice are exploring the familiar object. Interestingly, although the overall *Z* scores were found to be higher in Tat(–) mice, the fraction of active cells (Figures 4O and 4P) did not show any significant differences

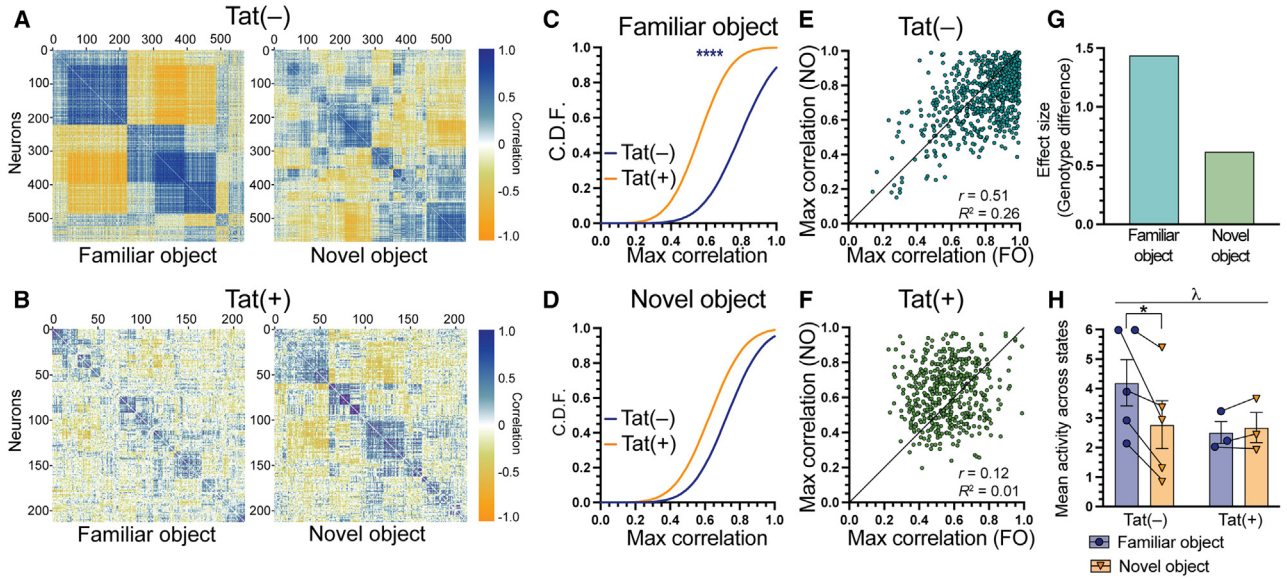

Figure 3. mPFC neurons are recruited during the NOR task and their activity reduces in the presence of the HIV-1 Tat protein

(A and B) Maximum cell-to-cell correlation matrices for familiar object (left) and novel object (right) from Tat(−) and Tat(+) mice, respectively.

(C) Cumulative distribution function plotting the maximum correlation frequency for familiar object for Tat(−) and Tat(+) mice. Kolmogorov-Smirnov test: genotype effect, ****$p < 0.0001$.

(D) Cumulative distribution function plotting the maximum correlation frequency for novel object for Tat(−) and Tat(+) mice. Kolmogorov-Smirnov test: N.S. $p > 0.05$.

(E) Scatterplot for Tat(−) mice ($n = 661$) with x axis and y axis showing maximum neuronal correlation while exploring the familiar and novel objects, respectively. Pearson correlation: $r = 0.51$, $p < 0.0001$.

(F) Scatterplot for Tat(+) mice ($n = 498$) with x axis and y axis showing maximum neuronal correlation while exploring the familiar and novel objects, respectively. Pearson correlation: $r = 0.12$, $p = 0.005$.

(G) Effects size of neurons for familiar (Cohen's $d = 1.44$) and novel object (Cohen's $d = 0.62$).

(H) Mean activity of neurons for Tat(−) and Tat(+) mice while exploring familiar and novel objects. Data presented as mean ± SEM. Two-way mixed ANOVA: genotype × object interaction $^{\lambda}p = 0.04$. Paired t test, Tat(−) mice: $^{*}p = 0.03$.

N.S., not significant; FO, familiar object; NO, novel object.

based on genotype and the type of object explored, which suggests that even though HIV-1 Tat affects the activity of cells, it does not affect the number of cells that are activated in the NOR task.

The upmodulated neurons in Tat(−) mice moderate recognition memory of the familiar object during the NOR task

An outline map from Tat(−) and Tat(+) mice with highlighted upmodulated (blue) and downmodulated (green) neurons during familiar object exploration was generated through peri-event analysis workflow in IDEAS (Figures 5A, 5B, and S4). Next, the up- and downmodulated neurons were extracted based on genotype and type of object being explored and were plotted 2 s pre- and post-object exploration with statistics performed at the following time points: −2, −1, 0, 1, and 2 s. For upmodulated neurons and familiar object exploration (Figure 5C), a two-way mixed ANOVA, with time as a within-subjects factor and genotype as a between-subjects factor, showed a main effect of time ($F(40, 2000) = 14.08$, $p < 0.001$), with the mean activity of upmodulated neurons increasing with time, and a main effect of genotype ($F(1, 50) = 1.61$, $p = 0.02$), with Tat(−) neurons displaying higher mean activity compared to neurons from Tat(+) mice. When analyzing separately for genotypes, a paired t test revealed that for both, Tat(−) mice (between −2 and 2 s, $t(34) = 6.14$, $p < 0.001$) and Tat(+) mice (between −2 and 2 s, $t(16) = 3.23$, $p = 0.005$), the mean activity of upmodulated neurons were significantly higher post- compared to pre-object exploration. Importantly, an interaction between time × genotype was found ($F(80, 2000) = 6.62$, $p < 0.001$), with upmodulated neurons increasing their mean activity for Tat(−) mice compared to Tat(+) mice when familiar object exploration started. This was confirmed, when considering the aforementioned time points and conducting independent t tests, which showed no differences in the mean activity of upmodulated neurons in Tat(−) and Tat(+) mice at −2 and −1 s; however the mean activity significantly increased in a time-dependent manner for Tat(−) mice compared to Tat(+) mice while exploring the familiar object (Figure 5C; 0 s, $t(50) = 2.20$, $p = 0.03$; 1 s, $t(50) = 3.53$, $p < 0.001$; 2 s, $t(50) = 3.21$, $p = 0.002$). Lastly, the mean Z score of the upmodulated neurons for Tat(−) mice during the familiar object exploration were significantly higher as compared to Tat(+) mice (Figure 5D; $t(50) = 2.42$, $p = 0.01$).

For downmodulated neurons and familiar object exploration (Figure 5E), a two-way mixed ANOVA showed a main effect of time ($F(40, 2120) = 4.34$, $p < 0.001$) and a main effect of genotype ($F(1, 53) = 1.91$, $p = 0.001$), with mean activity of downmodulated neurons decreasing with time and downmodulated neurons in

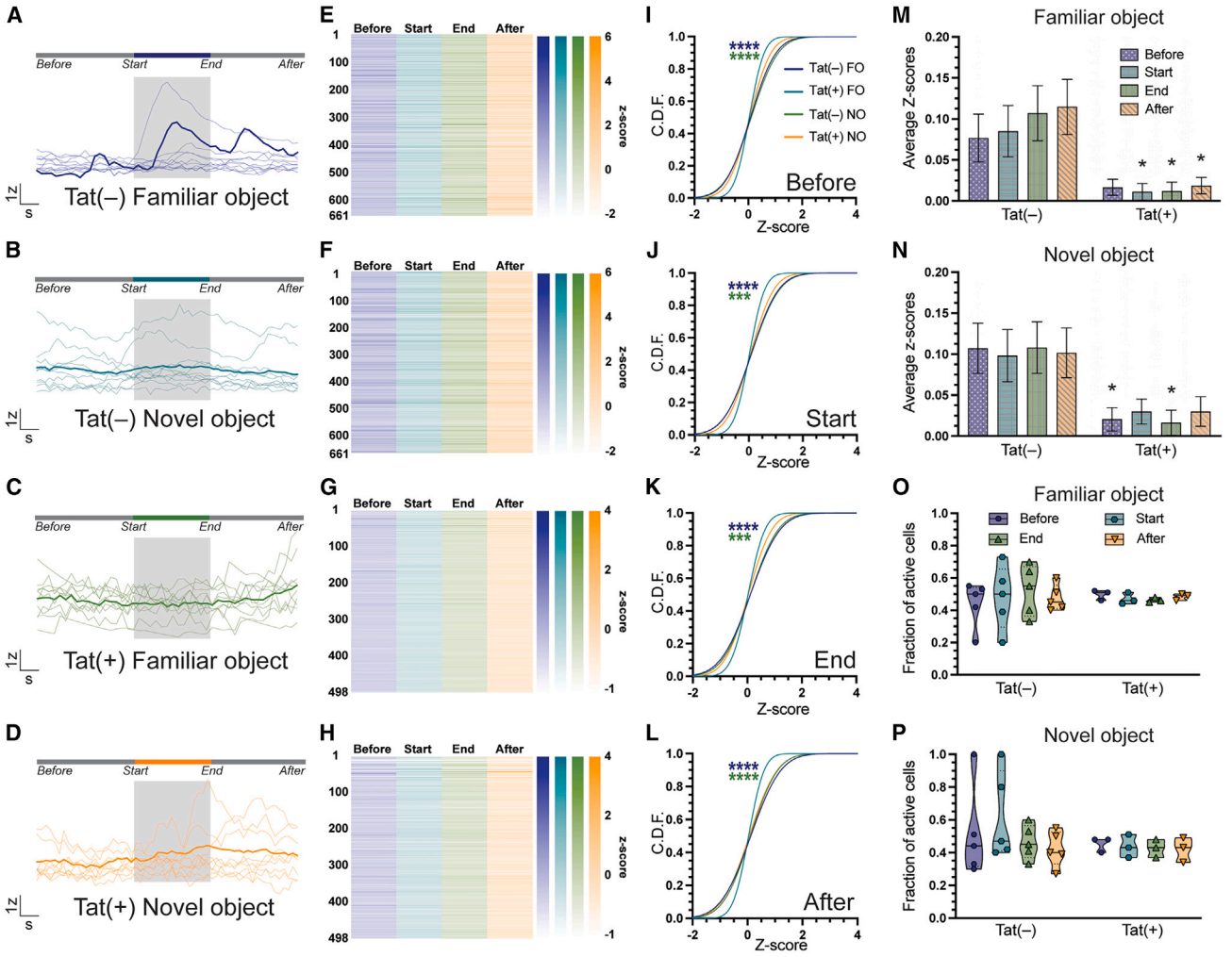

Figure 4. Neuronal activity in Tat(+) mice during all four epochs is reduced compared to Tat(−) mice in both familiar and novel objects exploration

(A–D) Neuronal traces of relative fluorescence changes (ΔF/F) in mPFC of Tat(−) mice during familiar (A) and novel (B) objects exploration and Tat(+) mice during familiar (C) and novel (D) objects exploration. Individual cell activity is indicated in lighter colors, with total average cell activity in darker colors and object exploration duration in the transparent gray block. Scale bars, x = time (in s variable per subject), y = *Z* score based on relative ΔF/F.

(E–H) *Z* scores shown as heat maps of the four epochs, *before* (blue), *start* of object exploration (teal), *end* of object exploration (green), and *after* (orange), of Tat(−) mice during familiar (E) and novel (F) objects exploration and Tat(+) mice during familiar (G) and novel (H) objects exploration.

(I) Cumulative distribution function for *before* epoch plotting the *Z* score frequency for familiar (Kolmogorov-Smirnov test: genotype effect, $^{****}p < 0.0001$) and novel (Kolmogorov-Smirnov test: genotype effect, $^{****}p < 0.0001$) object for Tat(−) and Tat(+) mice.

(J) Cumulative distribution function for *start* epoch plotting the *Z* score frequency for familiar (Kolmogorov-Smirnov test: genotype effect, $^{****}p < 0.0001$) and novel (Kolmogorov-Smirnov test: genotype effect, $^{***}p < 0.001$) objects for Tat(−) and Tat(+) mice.

(K) Cumulative distribution function for *end* epoch plotting the *Z* score frequency for familiar (Kolmogorov-Smirnov test: genotype effect, $^{****}p < 0.0001$) and novel (Kolmogorov-Smirnov test: genotype effect, $^{***}p < 0.001$) objects for Tat(−) and Tat(+) mice.

(L) Cumulative distribution function for *after* epoch plotting the *Z* score frequency for familiar (Kolmogorov-Smirnov test: genotype effect, $^{****}p < 0.0001$) and novel (Kolmogorov-Smirnov test: genotype effect, $^{****}p < 0.0001$) objects for Tat(−) and Tat(+) mice.

(M) Average *Z* score for Tat(−) and Tat(+) mice at different epochs, independent t test: *before* (N.S. $p > 0.05$), *start* ($^{*}p < 0.05$), *end* ($^{*}p < 0.05$), and *after* ($^{*}p < 0.05$), for familiar object exploration. Data presented as mean ± SEM.

(N) Average *Z* score for Tat(−) and Tat(+) mice at different epochs, independent t test: *before* ($^{*}p < 0.05$), *start* (N.S. $p > 0.05$), *end* ($^{*}p < 0.05$), and *after* (N.S. $p > 0.05$), for novel object exploration. Data presented as mean ± SEM.

(O and P) Fraction of active cells (*Z* score > 0) for Tat(−) and Tat(+) mice at different epochs, *before, start*, *end*, and *after*, for familiar (O) and novel (P) objects exploration. Data presented as mean ± SEM. Independent t test: N.S. for all epochs and objects $p > 0.05$.

N.S., not significant; C.D.F., cumulative distribution function; FO, familiar object; NO, novel object.

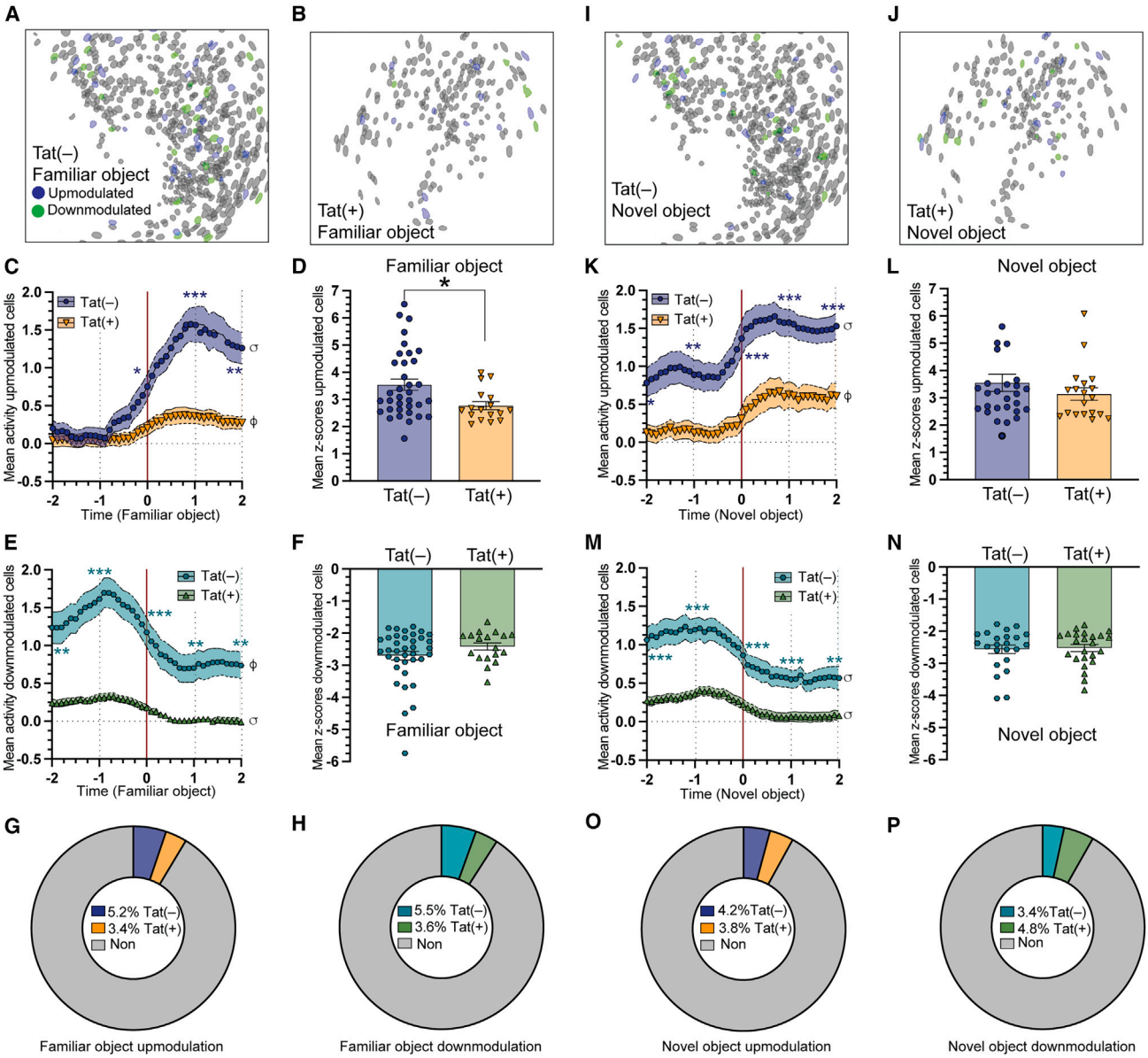

Figure 5. The upmodulated neurons in Tat(–) mice moderate recognition memory of the familiar object during the NOR task

(A and B) Outline of cells from a Tat(−) (A) and Tat(+) (B) mice while exploring the familiar object with highlighted upmodulated neurons (blue), downmodulated neurons (green), and nonmodulated neurons (gray).

(C) Peri-event analysis (−2 to 2 s) for upmodulated neurons in Tat(−) and Tat(+) mice when exploring familiar object. Independent t test genotype effect: −2 s (N.S. $p > 0.05$), −1 s (N.S. $p > 0.05$), 0 s ($^{*}p < 0.05$), 1 s ($^{***}p < 0.001$), 2 s ($^{**}p < 0.01$). Paired t test between −2 and 2 s: $^{\Phi}p < 0.05$, $^{\sigma}p < 0.001$.

(D) Mean *Z* scores of upmodulated neurons in Tat(−) and Tat(+) mice when exploring the familiar object. Data presented as mean ± SEM, independent t test: genotype effect: $^{*}p = 0.01$.

(E) Peri-event analysis (−2 to 2 s) for downmodulated neurons in Tat(−) and Tat(+) mice exploring the familiar object. Independent t test genotype effect: −2 s ($^{**}p < 0.01$), −1 s ($^{***}p < 0.001$), 0 s ($^{***}p < 0.001$), 1 s ($^{**}p < 0.01$), 2 s ($^{**}p < 0.01$). Paired t test between −2 and 2 s: $^{\Phi}p < 0.05$, $^{\sigma}p < 0.001$.

(F) Mean *Z* scores of downmodulated neurons in Tat(−) and Tat(+) mice when exploring the familiar object. Data presented as mean ± SEM, independent t test: genotype effect: N.S. $p > 0.05$.

(G and H) Percentage of up- (G) and downmodulated (H) neurons in Tat(−) and Tat(+) mice when exploring familiar object.

(I and J) Outline of cells from a Tat(−) (I) and Tat(+) (J) mice while exploring the novel object with highlighted upmodulated neurons (blue), downmodulated neurons (green), and nonmodulated neurons (gray).

(K) Peri-event analysis (−2 to 2 s) for upmodulated neurons in Tat(−) and Tat(+) mice when exploring novel object. Independent t test genotype effect: −2 s ($^{*}p < 0.05$), −1 s ($^{**}p < 0.01$), 0 s ($^{***}p < 0.001$), 1 s ($^{***}p < 0.001$), 2 s ($^{***}p < 0.01$). Paired t test between −2 and 2 s: $^{\Phi}p < 0.05$, $^{\sigma}p < 0.001$.

(L) Mean *Z* scores of upmodulated neurons in Tat(−) and Tat(+) mice when exploring the novel object. Data presented as mean ± SEM, independent t test: genotype effect: N.S. $p > 0.05$.

(legend continued on next page)

Tat(+) mice showing lower mean activity as compared to the neurons from Tat(−) mice, respectively. Separate analysis of Tat(−) and Tat(+) mice revealed that, for both, Tat(−) (between −2 and 2 s, $t(36) = -2.85$, $p = 0.007$) and Tat(+) mice (between −2 and 2 s, $t(17) = -4.46$, $p < 0.001$), the mean activity of downmodulated neurons were significantly lower post- compared to pre-object exploration. Additionally, an interaction between time × genotype ($F(80, 2120) = 9.05$, $p < 0.001$) revealed significance, with downmodulated neuron decreasing their mean activity more rapidly for Tat(−) mice when compared to Tat(+) mice around the onset of familiar object exploration. Note that the mean activity of downmodulated neurons at all five time points (Figure 5D; −2 s, $t(53) = 3.27$, $p = 0.02$; −1 s, $t(53) = 4.46$, $p < 0.001$; 0 s, $t(53) = 3.59$, $p < 0.001$; 1 s, $t(53) = 2.73$, $p = 0.008$; 2 s $t(50) = 3.98$, $p = 0.004$) was lower for Tat(+) mice as compared to Tat(−) mice when exploring the familiar object. Additionally, no differences in the mean *Z* score (Figure 5F) of the downmodulated neurons were found between Tat(−) and Tat(+) mice during familiar object exploration. Lastly, no significant differences were noted in the percentage of up- or downmodulated neurons (Figures 5G and 5H) in Tat(−) and Tat(+) mice during familiar object exploration.

The overall activity of up- and downmodulated neurons for novel object exploration is higher in Tat(−) mice compared to Tat(+) mice but does not moderate novel object recognition

An outline maps with highlighted upmodulated (blue) and downmodulated (green) neurons in Tat(−) and Tat(+)mice when the novel object was explored (Figures 5I, 5J, and S4). A two-way mixed ANOVA for upmodulated neurons during novel object exploration (Figure 5K) revealed a main effect of time ($F(40, 2000) = 19.57$, $p < 0.001$), with the mean activity of upmodulated neurons increasing with the object exploration duration. Further, a main effect of genotype was noted ($F(1, 50) = 3.61$, $p = 0.002$), with higher mean activity of upmodulated neurons in Tat(−) mice as compared to Tat(+) mice. A paired t test for each genotype separately showed that for both, Tat(−) mice (between −2 and 2 s, $t(27) = 5.41$, $p < 0.001$) and Tat(+) mice (between −2 and 2 s, $t(18) = 3.19$, $p = 0.005$), the mean activity of upmodulated neurons was significantly higher post- compared to pre-novel object exploration. Furthermore, two-way ANOVA also revealed a time × genotype interaction effect ($F(80, 1800) = 3.95$, $p < 0.001$), with upmodulated neurons in Tat(−) showing a more rapid increase in mean activity as compared with Tat(+) mice as time progressed during novel object exploration. Additionally, the mean activity of upmodulated neurons at −2, −1, 0, 1, and 2 s time points demonstrated significant genotype differences at all time points, with Tat(−) mice showing higher mean activity for upmodulated neurons as compared to Tat(+) mice when novel object was being explored (Figure 5K; −2 s, $t(45) = 2.67$, $p = 0.01$; −1 s $t(45) = 2.91$, $p = 0.005$; 0 s, $t(45) = 3.21$, $p = 0.002$; 1 s, $t(45) = 3.81$, $p < 0.001$; 2 s $t(45) = 3.65$, $p < 0.001$). Lastly, no differences in the mean *Z* score (Figure 5L) of upmodulated neurons were found for Tat(−) and Tat(+) mice during novel object exploration.

Finally, for downmodulated neurons and novel object exploration (Figure 5M), a two-way mixed ANOVA showed a main effect of time ($F(40, 1800) = 14.70$, $p < 0.001$), with mean activity of downmodulated neurons decreasing with time. Further, main effect of genotype was also observed ($F(1, 45) = 11.97$, $p < 0.001$), with downmodulated neurons in Tat(+) mice showing lower mean activity as compared to neurons from Tat(−) mice. Separate paired t tests for each genotype revealed that, for both, Tat(−) mice (between −2 and 2 s, $t(22) = -5.24$, $p < 0.001$) and Tat(+) mice (between −2 and 2 s, $t(23) = -3.54$, $p < 0.001$), the mean activity of downmodulated neurons were significantly lower post-compared to pre-novel object exploration. Furthermore, an interaction between time × genotype ($F(80, 1800) = 23.49$, $p < 0.001$) revealed a significance, with downmodulated neuron showing a steeper decrease in their mean activity for Tat(−) mice when compared to Tat(+) mice around the onset of exploration of the novel object. Note that the mean activity of downmodulated neurons at all five time points (Figure 5M; −2 s, $t(45) = 4.84$, $p < 0.001$; −1 s, $t(45) = 5.25$, $p < 0.001$; 0 s, $t(45) = 4.27$, $p < 0.001$; 1 s, $t(45) = 3.17$, $p < 0.001$; 2 s, $t(45) = 2.99$, $p = 0.004$) was lower for both Tat(+) mice as compared to Tat(−) mice when exploring the novel object. Additionally, no differences in the mean *Z* score (Figure 5N) of the downmodulated neurons were found between Tat(−) and Tat(+) mice during novel object exploration. Finally, no significant differences were noted in the percentage of up- or downmodulated neurons (Figures 5O and 5P) in Tat(−) and Tat(+) mice while exploring the novel object.

DISCUSSION

Recognition memory is based on the judgment about previously occurred stimuli, which is based on the relative familiarity or novelty of individual objects and analyzing recency information.[89] Decades of studies have highlighted the importance of the perirhinal cortex in recognition memory and discrimination of objects.[90–95] However, the role of the mPFC in recognition memory should not be undermined. Numerous electrophysiological and behavioral evidence have shown that mPFC neurons carry information regarding recognition and recency discrimination,[63] which is disrupted with damage to this region.[64–67] The HIV-1 protein Tat causes significant changes in PFC neurons with studies from our lab showing Tat-induced neuronal activity changes in the PFC, as well as deficits in PFC-related behavioral tasks in HIV-1 Tat transgenic mice.[60,96–100] Although there are plethora of information with regards to behavioral and

(M) Peri-event analysis (−2 to 2 s) for downmodulated neurons in Tat(−) and Tat(+) mice exploring the novel object. Independent t test genotype effect: −2 s (***$p < 0.001$), −1 s (***$p < 0.001$), 0 s (***$p < 0.001$), 1 s (***$p < 0.001$), 2 s (**$p < 0.01$). Paired t test between −2 and 2 s: $^{\alpha}p < 0.001$.
(N) Mean *Z* scores of downmodulated neurons in Tat(−) and Tat(+) mice when exploring the novel object. Data presented as mean ± SEM, independent t test: genotype effect: N.S. $p > 0.05$.
(O and P) Percentage of up- (O) and downmodulated (P) neurons in Tat(−) and Tat(+) mice when exploring the novel object.
N.S., not significant; Non, nonmodulated.

electrophysiology studies, it is unclear how PFC neurons support the discrimination of familiarity versus novelty at the cellular level. Therefore, the goal of the present study was 2-fold, first, to quantify neuronal activity during exploration of a familiar object versus a novel object, and second, to assess how Tat expression alters neuronal activity during object exploration.

For the behavioral task, we utilized the NOR task to assess recognition memory in our HIV-1 Tat transgenic mouse model, which predominantly involves the mPFC.[101] Tat expression in mice has typically been demonstrated to induce deficiencies in NOR learning and memory,[54,102] which is supported by the current study when additional animals were added (Figures 2E and 2F). To further substantiate our findings, past studies from our lab have shown trends with Tat(−) mice preferring to explore the novel object over the familiar object, whereas Tat(+) mice showed no discrimination.[60–62] The lack of behavioral differences in the present study when only considering GCaMP injected mice may be due to low number of animals used in the study. Additionally, previous studies have shown sex-specific effects in the NOR task, with female mice showing object discrimination,[60] whereas Tat(−) males were not able to successfully discriminate between familiar and novel objects.[61] Therefore, it is necessary to include female Tat transgenic mice in future *in vivo* calcium imaging studies to further assess if these sex-specific behavioral differences extend to neuronal alterations as well. Another interesting finding is the observation that Tat(−) and Tat(+) mice show differential exploration patterns (Figures 2C and 2D), with decreased center zone exploration and increased time spent in the corners for Tat(+) mice as compared to Tat(−) mice, which may be due to increased anxiety-like behavior in the presence of Tat.[56,57,62,103] Although the neuronal data from the center zone were not analyzed in the present study, this observation lays a strong foundation for a potential future study; to evaluate how PFC projecting neurons to the amygdala (PFC→amygdala circuitry, with the aid of retrograde tracers),[104,105] are affected by Tat expression during an anxiety-related task, since anxiety-like disorders are highly prevalent in PLWH.[106,107]

Past calcium imaging studies have shown mixed results with increased,[108] decreased,[109,110] or no change[111] in calcium activity to a familiar stimulus. Here, we report that during exploration of the familiar object, neuronal calcium activity was increased in control Tat(−) mice but not transgenic Tat(+) mice. Further, the neurons in Tat(−) mice were highly correlated during familiar object exploration as compared to novel object exploration, as seen by clustering of neurons in the correlation matrix (Figure 3A). This suggests that there is higher synchronization of neuronal firing in Tat(−) mice during exploration of the familiar object, which may be due to the recollection of the previous encounter with that object. Interestingly, the clustering of the neurons in Tat(−) mice were not observed during the novel object exploration, potentially as it was the first encounter with that "novel" object and repeated encounter with the same object may increase neuronal correlation and synchrony. Previous imaging studies in PLWH with HAND symptoms have shown that there is a significant decrease in salience and executive networks despite viral suppression in both plasma and cerebrospinal fluid (CSF), with resting-state fMRI showing decreased connectivity and reduced synchronicity in neurons.[112] Additionally, studies have also shown that HIV-1 infection alters functional connectivity and reorganizes brain network, which leads to cognitive decline.[113,114] In line with these past studies, the current study showed that in the presence of Tat expression (Figure 3B), regardless of what object was being explored, the correlation and synchrony of neuronal activity were reduced compared to Tat(−) mice. This may suggest that Tat(+) mice lacked the ability to discriminate between familiar and novel objects, which could arise from disruption of functional connectivity due to Tat expression.

In addition to analyzing calcium activity of mPFC neurons in the NOR task overall, we divided object exploration behavior in four different epochs (*before*, *start*, *end*, and *after*) to assess if mPFC neuronal activity changes across these time points and importantly in the presence of Tat expression. In relation to familiar object exploration (Figure 4M) it was observed that for the average *Z* score when approaching the object, i.e., *before* epoch, there was no significant difference between Tat(−) and Tat(+) mice; however, significant differences for genotype was observed across time points; only Tat(−) mice demonstrated a time-dependent effect, with the highest *Z* score found for *after* epoch followed by *end*, *start*, and *before* epoch. This outcome suggests that although the *Z* score when approaching the object is similar between Tat(−) and Tat(+) mice, neuronal activity steadily increases in Tat(−) mice with exploratory behavior. This suggests that mPFC neurons as a whole are involved in all phases of recognition memory and memory retrieval, which is disrupted in the presence of Tat. It is known that mPFC neurons project to various cortical and subcortical regions[115] forming their own subpopulation,[116–118] thus, there is a possibility that each epoch activity might be mediated by mPFC neurons projecting to a distinct CNS regions. To assess this possibility, it would be exciting for future studies to analyze the cells that are specifically upmodulated at these time points and see if they form distinct subpopulations or if they overlap with each other. Interestingly, the same pattern of increase in the neuronal activity across epochs was not observed in either Tat(−) or Tat(+) mice when exploring the novel object (Figure 4N) and remained the same across all epochs.

Another surprising finding was that Tat expression did not affect number of activated neurons during the four epoch time points (Figures 4O and 5P). Even though the overall neuronal activity in Tat(+) animals was significantly reduced, the number of cells that were activated remained the same as for Tat(−) mice, suggesting that Tat expression causes neuronal dysfunction but does not necessarily alter how many neurons are active. This finding is in line with past literature that have shown that Tat exerts its effects directly by altering NMDR function[26–28] and indirectly by promoting the release of proinflammatory cytokines via glia cells.[30,32] Moreover, we conducted perievent analysis specifically on up- and downmodulated neurons (Figure 5). Overall, it was found that the mean neuronal activity for Tat(−) mice during familiar and novel objects exploration were significantly higher than for Tat(+) mice. Similar to the epoch time points data, the activity in upmodulated neurons in Tat(−) mice increased in a time-dependent manner, which was also observed for the upmodulated neurons in Tat(+) mice; however, only with a small change as compared to Tat(−) mice, which

further provides insight into Tat's mechanism of action. With regards to the outline maps of the cells with highlighted up- and downmodulated cells (Figures 5A, 5B, 5I, and 5J), it is essential to note that subpopulation of up- and downmodulated cells during familiar and novel objects exploration in both Tat(−) and Tat(+) mice are distinct with hardly any overlapping cells. This is an important finding as it further strengthens our line of thought that mPFC may have different subpopulations of cells and form different memory engrams for a particular object/memory with the support engram cells from other brain regions.[119] Memory engrams are composed of micro- and macro-circuits from numerous cell ensembles, brain regions and both inhibitory and excitatory neurons leading to creation of memory specific engrams.[119–121] The results from the present study have pivoted us to expand our research further with the help of dual-color *in vivo* calcium imaging along with optogenetics. Using these sophisticated tools, we could identify the subpopulation of cells that are projecting from mPFC to other brain regions that are critical for memory formation, retrieval, and consolidation, and optogenetically manipulate these cells to make the mice choose between objects/tasks in order to assess in detail how the mPFC neuronal subpopulations aid in the formation of memory engrams.

Another point to consider is that the GCaMP construct used in the present study is non-specific and labels both pyramidal and interneurons. As differential effects of Tat have been shown with inhibitory versus excitatory neurons,[96] future studies should use neuronal subtype-specific virus as reported by a previous study that focused on a calcium sensor that only targets excitatory neurons in the mPFC.[122] Moreover, past studies have shown that in addition to HIV-1 Tat's effects on the PFC, Tat also affects other CNS regions such as anterior cingulate cortex, amygdala, nucleus accumbens, and dentate gyrus.[32,123] These effects have been shown to be mediated by neuronal excititoxicity and activation of microglia.[30–32] Thus, to build on these findings, future studies should also investigate and trace various mPFC circuitries, including the PFC→amygdala,[42,43] hippocampus→PFC,[124,125] and PFC→entorhinal cortex[126] pathways, to assess their roles in working memory tasks and the interplay of different circuitries involved in memory processing. Lastly, HAND is recognized as an inflammatory disease, with enhanced gliosis and neuroinflammatory response playing a pivotal role in neuronal injury.[30–35] A recent histological study from our lab demonstrated that HIV-1 infection in the humanized bone marrow/liver/thymus (BLT) mouse model, led to HIV-infected human cells into the brain that increased glial fibrillary acidic protein (GFAP) expression and heightened presence of Iba-1+ microglia across various CNS regions, highlighting the extent of HIV-1-induced neuroinflammation and HIV neuroinvasion.[125] Consequently, future research should focus on elucidating the dynamic interactions between glial cells and neurons, leveraging *in vivo* calcium imaging techniques as demonstrated by recent advancements in the field.[127–129]

In summary, while the activity and synchronized firing patterns of mPFC neurons are significantly reduced during object exploration in the presence of Tat, the number of activated cells remains unchanged. Based on the results from the present study it is suggested that the relationship between behavior and neuronal activity is not always linear. The NOR task relies on an animal's innate exploratory behavior, where it is expected that the animal will naturally explore the novel object due to its novelty.[130–132] Therefore, it is not farfetched to hypothesize that neuronal firing rate would be higher when the animal explores the novel object. On the contrary, we found that it is the "familiarity" that drives increased neuronal activity. The mPFC neurons in "healthy" mice contribute to recognition memory with neuronal firing being more robust when encountering familiar object, essentially acting as "recognition cells." This outcome are in line with a previous study suggesting that familiarity increases brain activity in numerous brain regions including the perirhinal cortex, and the left ventrolateral and anteromedial frontal cortex.[133] Based on the neuronal data from the present study, an important question is if the NOR task should be redefined as the "familiar object recognition" task?

Limitations of the study

There are several limitations in the present study. First, we intentionally selected male mice for GCaMP and GRIN lens implantation due to their larger size as handling larger male mice was more practical for the extended survival surgery. As this protocol is now established in our lab, all future studies to assess neuronal activity will include female Tat transgenic mice to investigate sex differences and their impact on memory. Second, the Tat transgenic mouse model used in the present study expresses only one of the HIV-1 proteins. Although, this is a well-established representation of neuroHIV, different viral proteins may interact with numerous signaling pathways, which could affect the CNS and behavior in different ways compared to a single protein; therefore, it is important to consider this limitation when generalizing findings to PLWH. To overcome this limitation, future *in vivo* calcium imaging studies should consider using either EcoHIV infected mice[134,135] or even HIV infection in humanized mouse models.[136,137] Finally, the use of doxycycline to induce Tat expression in the Tat transgenic mouse model is considered a limitation, as it has been shown that doxycycline itself can exert neuroprotective effects.[138] Hence, to address this caveat and minimize bias even the Tat(−) mice were placed on doxycycline-enriched chow throughout the study.

RESOURCE AVAILABILITY

Lead contact

Further information and requests for resources and reagents should be directed to and will be fulfilled by the lead contact, Sylvia Fitting (sfitting@email.unc.edu).

Material availability

This study did not generate new unique reagents.

Data and code availability

- Behavioral annotations and raw data from CNMF-E and *in vivo* calcium imaging reported in this paper are publicly available on Mendeley Data as of the date of publication (https://doi.org/10.17632/62z7892yr9.1).
- This paper does not report any original code.
- Any additional information required to reanalyze the data reported in this paper is available from the lead contact upon request.

ACKNOWLEDGMENTS

We thank Douglas Kim and GENIE Project for the GCaMP6f virus and plasmid; Shanna Resendez, Waylin Yu, and Srinivas Gorur-Shandilya, Inscopix, for their assistance with the survival surgery and calcium recording and IDEAS platform; and animal care technician Patrick Stutts for maintaining the welfare of our animals throughout the study. This work was supported by grants R21-DA057871 and R01-DA055523 from NIDA (PI, S.F.).

AUTHOR CONTRIBUTIONS

Conceptualization, B.J.Y.-S. and S.F.; data curation, B.J.Y.-S. and S.F.; formal analysis, B.J.Y.-S., A.P.Y., R.P.P., and S.F.; funding acquisition, S.F.; investigation, B.J.Y.-S., A.P.Y., R.P.P., and S.F.; methodology, B.J.Y.-S., R.P.P., and S.F.; project administration, B.J.Y.-S. and S.F.; software, B.J.Y.-S., A.P.Y., and S.F.; supervision, S.F.; validation, B.J.Y.-S., A.P.Y., R.P.P., and S.F.; visualization, B.J.Y.-S., A.P.Y., and S.F.; writing – original draft, B.J.Y.-S. and S.F.; writing – review and editing, B.J.Y.-S., A.P.Y., R.P.P., and S.F.

DECLARATION OF INTERESTS

The authors declare no competing interests.

STAR★METHODS

Detailed methods are provided in the online version of this paper and include the following:

- KEY RESOURCES TABLE
- EXPERIMENTAL MODEL AND STUDY PARTICIPANT DETAILS
  - Mice
  - Ethical approval declaration
- METHOD DETAILS
  - Virus
  - Stereotaxic surgery and viral injection
  - Lens implant
  - Behavior
  - Calcium recording
  - Preprocessing
  - Spatial bandpass filter
  - Motion correction
  - Project movie
  - ΔF/F
  - CNMF-E
  - Event detection
  - Calcium imaging QC report
  - Compare neural activity across states
  - Compare neural circuit correlations across states
  - Peri-event analysis
  - Combine and compare correlation data
  - Combine and compare population activity data
  - Combine and compare peri-event analysis data
- QUANTIFICATION AND STATISTICAL ANALYSIS

SUPPLEMENTAL INFORMATION

Supplemental information can be found online at https://doi.org/10.1016/j.isci.2025.112075.

Received: October 28, 2024
Revised: December 20, 2024
Accepted: February 17, 2025
Published: February 22, 2025

REFERENCES

1. Bekker, L.G., Beyrer, C., Mgodi, N., Lewin, S.R., Delany-Moretlwe, S., Taiwo, B., Masters, M.C., and Lazarus, J.V. (2023). HIV infection. Nat. Rev. Dis. Primers *9*, 42. https://doi.org/10.1038/s41572-023-00452-3.

2. An, S.F., Groves, M., Gray, F., and Scaravilli, F. (1999). Early entry and widespread cellular involvement of HIV-1 DNA in brains of HIV-1 positive asymptomatic individuals. J. Neuropathol. Exp. Neurol. *58*, 1156–1162. https://doi.org/10.1097/00005072-199911000-00005.

3. Honeycutt, J.B., Wahl, A., Baker, C., Spagnuolo, R.A., Foster, J., Zakharova, O., Wietgrefe, S., Caro-Vegas, C., Madden, V., Sharpe, G., et al. (2016). Macrophages sustain HIV replication *in vivo* independently of T cells. J. Clin. Investig. *126*, 1353–1366. https://doi.org/10.1172/JCI84456.

4. Joseph, S.B., Arrildt, K.T., Sturdevant, C.B., and Swanstrom, R. (2015). HIV-1 target cells in the CNS. J. Neurovirol. *21*, 276–289. https://doi.org/10.1007/s13365-014-0287-x.

5. Schnell, G., Joseph, S., Spudich, S., Price, R.W., and Swanstrom, R. (2011). HIV-1 replication in the central nervous system occurs in two distinct cell types. PLoS Pathog. *7*, e1002286. https://doi.org/10.1371/journal.ppat.1002286.

6. McRae, M. (2016). HIV and viral protein effects on the blood brain barrier. Tissue Barriers *4*, e1143543. https://doi.org/10.1080/21688370.2016.1143543.

7. Brack-Werner, R. (1999). Astrocytes: HIV cellular reservoirs and important participants in neuropathogenesis. AIDS *13*, 1–22. https://doi.org/10.1097/00002030-199901140-00003.

8. Churchill, M.J., Wesselingh, S.L., Cowley, D., Pardo, C.A., McArthur, J.C., Brew, B.J., and Gorry, P.R. (2009). Extensive astrocyte infection is prominent in human immunodeficiency virus-associated dementia. Ann. Neurol. *66*, 253–258. https://doi.org/10.1002/ana.21697.

9. Kramer-Hammerle, S., Rothenaigner, I., Wolff, H., Bell, J.E., and Brack-Werner, R. (2005). Cells of the central nervous system as targets and reservoirs of the human immunodeficiency virus. Virus Res. *111*, 194–213. https://doi.org/10.1016/j.virusres.2005.04.009.

10. Lane, J.H., Sasseville, V.G., Smith, M.O., Vogel, P., Pauley, D.R., Heyes, M.P., and Lackner, A.A. (1996). Neuroinvasion by simian immunodeficiency virus coincides with increased numbers of perivascular macrophages/microglia and intrathecal immune activation. J. Neurovirol. *2*, 423–432. https://doi.org/10.3109/13550289609146909.

11. Osborne, O., Peyravian, N., Nair, M., Daunert, S., and Toborek, M. (2020). The paradox of HIV blood-brain barrier penetrance and antiretroviral drug delivery deficiencies. Trends Neurosci. *43*, 695–708. https://doi.org/10.1016/j.tins.2020.06.007.

12. Heaton, R.K., Clifford, D.B., Franklin, D.R., Jr., Woods, S.P., Ake, C., Vaida, F., Ellis, R.J., Letendre, S.L., Marcotte, T.D., Atkinson, J.H., et al. (2010). HIV-associated neurocognitive disorders persist in the era of potent antiretroviral therapy: CHARTER Study. Neurology *75*, 2087–2096. https://doi.org/10.1212/WNL.0b013e318200d727.

13. Wang, Y., Liu, M., Lu, Q., Farrell, M., Lappin, J.M., Shi, J., Lu, L., and Bao, Y. (2020). Global prevalence and burden of HIV-associated neurocognitive disorder: A meta-analysis. Neurology *95*, e2610–e2621. https://doi.org/10.1212/WNL.0000000000010752.

14. Reger, M., Welsh, R., Razani, J., Martin, D.J., and Boone, K.B. (2002). A meta-analysis of the neuropsychological sequelae of HIV infection. J. Int. Neuropsychol. Soc. *8*, 410–424. https://doi.org/10.1017/s1355617702813212.

15. Dore, G.J., Correll, P.K., Li, Y., Kaldor, J.M., Cooper, D.A., and Brew, B.J. (1999). Changes to AIDS dementia complex in the era of highly active antiretroviral therapy. AIDS *13*, 1249–1253. https://doi.org/10.1097/00002030-199907090-00015.

16. Ellis, R., Langford, D., and Masliah, E. (2007). HIV and antiretroviral therapy in the brain: neuronal injury and repair. Nat. Rev. Neurosci. *8*, 33–44. https://doi.org/10.1038/nrn2040.

17. Gannon, P., Khan, M.Z., and Kolson, D.L. (2011). Current understanding of HIV-associated neurocognitive disorders pathogenesis. Curr. Opin. Neurol. *24*, 275–283. https://doi.org/10.1097/WCO.0b013e32834695fb.

18. Heaton, R.K., Franklin, D.R., Ellis, R.J., McCutchan, J.A., Letendre, S.L., Leblanc, S., Corkran, S.H., Duarte, N.A., Clifford, D.B., Woods, S.P., et al. (2011). HIV-associated neurocognitive disorders before and during the era of combination antiretroviral therapy: differences in rates, nature, and predictors. J. Neurovirol. *17*, 3–16. https://doi.org/10.1007/s13365-010-0006-1.

19. Hardy, D.J., and Vance, D.E. (2009). The neuropsychology of HIV/AIDS in older adults. Neuropsychol. Rev. *19*, 263–272. https://doi.org/10.1007/s11065-009-9087-0.

20. Garvey, L.J., Yerrakalva, D., and Winston, A. (2009). Correlations between computerized battery testing and a memory questionnaire for identification of neurocognitive impairment in HIV type 1-infected subjects on stable antiretroviral therapy. AIDS Res. Hum. Retroviruses *25*, 765–769. https://doi.org/10.1089/aid.2008.0292.

21. Cysique, L.A., Maruff, P., and Brew, B.J. (2004). Prevalence and pattern of neuropsychological impairment in human immunodeficiency virus-infected/acquired immunodeficiency syndrome (HIV/AIDS) patients across pre- and post-highly active antiretroviral therapy eras: a combined study of two cohorts. J. Neurovirol. *10*, 350–357. https://doi.org/10.1080/13550280490521078.

22. Johnson, T.P., Patel, K., Johnson, K.R., Maric, D., Calabresi, P.A., Hasbun, R., and Nath, A. (2013). Induction of IL-17 and nonclassical T-cell activation by HIV-Tat protein. Proc. Natl. Acad. Sci. USA *110*, 13588–13593. https://doi.org/10.1073/pnas.1308673110.

23. Gaskill, P.J., Miller, D.R., Gamble-George, J., Yano, H., and Khoshbouei, H. (2017). HIV, Tat and dopamine transmission. Neurobiol. Dis. *105*, 51–73. https://doi.org/10.1016/j.nbd.2017.04.015.

24. Dickens, A.M., Yoo, S.W., Chin, A.C., Xu, J., Johnson, T.P., Trout, A.L., Hauser, K.F., and Haughey, N.J. (2017). Chronic low-level expression of HIV-1 Tat promotes a neurodegenerative phenotype with aging. Sci. Rep. *7*, 7748. https://doi.org/10.1038/s41598-017-07570-5.

25. Nath, A., and Steiner, J. (2014). Synaptodendritic injury with HIV-Tat protein: What is the therapeutic target? Exp. Neurol. *251*, 112–114. https://doi.org/10.1016/j.expneurol.2013.11.004.

26. Longordo, F., Feligioni, M., Chiaramonte, G., Sbaffi, P.F., Raiteri, M., and Pittaluga, A. (2006). The human immunodeficiency virus-1 protein transactivator of transcription up-regulates N-methyl-D-aspartate receptor function by acting at metabotropic glutamate receptor 1 receptors coexisting on human and rat brain noradrenergic neurones. J. Pharmacol. Exp. Therapeut. *317*, 1097–1105. https://doi.org/10.1124/jpet.105.099630.

27. Song, L., Nath, A., Geiger, J.D., Moore, A., and Hochman, S. (2003). Human immunodeficiency virus type 1 Tat protein directly activates neuronal N-methyl-D-aspartate receptors at an allosteric zinc-sensitive site. J. Neurovirol. *9*, 399–403. https://doi.org/10.1080/13550280390201704.

28. Wang, P., Barks, J.D., and Silverstein, F.S. (1999). Tat, a human immunodeficiency virus-1-derived protein, augments excitotoxic hippocampal injury in neonatal rats. Neuroscience *88*, 585–597. https://doi.org/10.1016/s0306-4522(98)00242-5.

29. Chandra, T., Maier, W., König, H.G., Hirzel, K., Kögel, D., Schüler, T., Chandra, A., Demirhan, I., and Laube, B. (2005). Molecular interactions of the type 1 human immunodeficiency virus transregulatory protein Tat with N-methyl-d-aspartate receptor subunits. Neuroscience *134*, 145–153. https://doi.org/10.1016/j.neuroscience.2005.02.049.

30. Chen, P., Mayne, M., Power, C., and Nath, A. (1997). The Tat protein of HIV-1 induces tumor necrosis factor-alpha production. Implications for HIV-1-associated neurological diseases. J. Biol. Chem. *272*, 22385–22388. https://doi.org/10.1074/jbc.272.36.22385.

31. Ajasin, D., and Eugenin, E.A. (2020). HIV-1 Tat: Role in Bystander Toxicity. Front. Cell Infect Microbiol. *10*, 61. https://doi.org/10.3389/fcimb.2020.00061.

32. Paris, J.J., Singh, H.D., Carey, A.N., and McLaughlin, J.P. (2015). Exposure to HIV-1 Tat in brain impairs sensorimotor gating and activates microglia in limbic and extralimbic brain regions of male mice. Behav. Brain Res. *291*, 209–218. https://doi.org/10.1016/j.bbr.2015.05.021.

33. Masliah, E., Heaton, R.K., Marcotte, T.D., Ellis, R.J., Wiley, C.A., Mallory, M., Achim, C.L., McCutchan, J.A., Nelson, J.A., Atkinson, J.H., and Grant, I. (1997). Dendritic injury is a pathological substrate for human immunodeficiency virus-related cognitive disorders. HNRC Group. The HIV Neurobehavioral Research Center. Ann. Neurol. *42*, 963–972. https://doi.org/10.1002/ana.410420618.

34. Haughey, N.J., Nath, A., Mattson, M.P., Slevin, J.T., and Geiger, J.D. (2001). HIV-1 Tat through phosphorylation of NMDA receptors potentiates glutamate excitotoxicity. J. Neurochem. *78*, 457–467. https://doi.org/10.1046/j.1471-4159.2001.00396.x.

35. Hu, X.T. (2016). HIV-1 Tat-Mediated Calcium Dysregulation and Neuronal Dysfunction in Vulnerable Brain Regions. Curr. Drug Targets *17*, 4–14. https://doi.org/10.2174/1389450116666150531162212.

36. Capone, C., Cervelli, M., Angelucci, E., Colasanti, M., Macone, A., Mariottini, P., and Persichini, T. (2013). A role for spermine oxidase as a mediator of reactive oxygen species production in HIV-Tat-induced neuronal toxicity. Free Radic. Biol. Med. *63*, 99–107. https://doi.org/10.1016/j.freeradbiomed.2013.05.007.

37. Samikkannu, T., Atluri, V.S.R., Arias, A.Y., Rao, K.V.K., Mulet, C.T., Jayant, R.D., and Nair, M.P.N. (2014). HIV-1 subtypes B and C Tat differentially impact synaptic plasticity expression and implicates HIV-associated neurocognitive disorders. Curr. HIV Res. *12*, 397–405. https://doi.org/10.2174/1570162x13666150121104720.

38. Haughey, N.J., Holden, C.P., Nath, A., and Geiger, J.D. (1999). Involvement of inositol 1,4,5-trisphosphate-regulated stores of intracellular calcium in calcium dysregulation and neuron cell death caused by HIV-1 protein tat. J. Neurochem. *73*, 1363–1374. https://doi.org/10.1046/j.1471-4159.1999.0731363.x.

39. Mattson, M.P., Haughey, N.J., and Nath, A. (2005). Cell death in HIV dementia. Cell Death Differ. *12*, 893–904. https://doi.org/10.1038/sj.cdd.4401577.

40. Fitting, S., Knapp, P.E., Zou, S., Marks, W.D., Bowers, M.S., Akbarali, H.I., and Hauser, K.F. (2014). Interactive HIV-1 Tat and morphine-induced synaptodendritic injury is triggered through focal disruptions in Na^+ influx, mitochondrial instability, and Ca^{2+} overload. J. Neurosci. *34*, 12850–12864. https://doi.org/10.1523/JNEUROSCI.5351-13.2014.

41. Chang, L., Ernst, T., Leonido-Yee, M., Witt, M., Speck, O., Walot, I., and Miller, E.N. (1999). Highly active antiretroviral therapy reverses brain metabolite abnormalities in mild HIV dementia. Neurology *53*, 782–789. https://doi.org/10.1212/wnl.53.4.782.

42. Chang, L., and Shukla, D.K. (2018). Imaging studies of the HIV-infected brain. Handb. Clin. Neurol. *152*, 229–264. https://doi.org/10.1016/B978-0-444-63849-6.00018-9.

43. Ances, B.M., and Hammoud, D.A. (2014). Neuroimaging of HIV-associated neurocognitive disorders (HAND). Curr. Opin. HIV AIDS *9*, 545–551. https://doi.org/10.1097/COH.0000000000000112.

44. Hakkers, C.S., Arends, J.E., Barth, R.E., Du Plessis, S., Hoepelman, A.I.M., and Vink, M. (2017). Review of functional MRI in HIV: effects of aging and medication. J. Neurovirol. *23*, 20–32. https://doi.org/10.1007/s13365-016-0483-y.

45. Masters, M.C., and Ances, B.M. (2014). Role of neuroimaging in HIV-associated neurocognitive disorders. Semin. Neurol. *34*, 89–102. https://doi.org/10.1055/s-0034-1372346.

46. Thompson, P.M., and Jahanshad, N. (2015). Novel Neuroimaging Methods to Understand How HIV Affects the Brain. Curr. HIV AIDS Rep. *12*, 289–298. https://doi.org/10.1007/s11904-015-0268-6.

47. Connolly, C.G., Bischoff-Grethe, A., Jordan, S.J., Woods, S.P., Ellis, R.J., Paulus, M.P., and Grant, I.; Translational Methamphetamine AIDS Research Center TMARC Group (2014). Altered functional response to risky choice in HIV infection. PLoS One *9*, e111583. https://doi.org/10.1371/journal.pone.0111583.

48. Plessis, S.D., Vink, M., Joska, J.A., Koutsilieri, E., Stein, D.J., and Emsley, R. (2014). HIV infection and the fronto-striatal system: a systematic review and meta-analysis of fMRI studies. AIDS *28*, 803–811. https://doi.org/10.1097/QAD.0000000000000151.

49. Vaghi, M.M., Vértes, P.E., Kitzbichler, M.G., Apergis-Schoute, A.M., van der Flier, F.E., Fineberg, N.A., Sule, A., Zaman, R., Voon, V., Kundu, P., et al. (2017). Specific Frontostriatal Circuits for Impaired Cognitive Flexibility and Goal-Directed Planning in Obsessive-Compulsive Disorder: Evidence From Resting-State Functional Connectivity. Biol. Psychiatry *81*, 708–717. https://doi.org/10.1016/j.biopsych.2016.08.009.

50. Bruce-Keller, A.J., Turchan-Cholewo, J., Smart, E.J., Geurin, T., Chauhan, A., Reid, R., Xu, R., Nath, A., Knapp, P.E., and Hauser, K.F. (2008). Morphine causes rapid increases in glial activation and neuronal injury in the striatum of inducible HIV-1 Tat transgenic mice. Glia *56*, 1414–1427. https://doi.org/10.1002/glia.20708.

51. Hauser, K.F., Hahn, Y.K., Adjan, V.V., Zou, S., Buch, S.K., Nath, A., Bruce-Keller, A.J., and Knapp, P.E. (2009). HIV-1 Tat and morphine have interactive effects on oligodendrocyte survival and morphology. Glia *57*, 194–206. https://doi.org/10.1002/glia.20746.

52. Fitting, S., Ignatowska-Jankowska, B.M., Bull, C., Skoff, R.P., Lichtman, A.H., Wise, L.E., Fox, M.A., Su, J., Medina, A.E., Krahe, T.E., et al. (2013). Synaptic dysfunction in the hippocampus accompanies learning and memory deficits in human immunodeficiency virus type-1 Tat transgenic mice. Biol. Psychiatry *73*, 443–453. https://doi.org/10.1016/j.biopsych.2012.09.026.

53. Fitting, S., Xu, R., Bull, C., Buch, S.K., El-Hage, N., Nath, A., Knapp, P.E., and Hauser, K.F. (2010). Interactive comorbidity between opioid drug abuse and HIV-1 Tat: chronic exposure augments spine loss and sublethal dendritic pathology in striatal neurons. Am. J. Pathol. *177*, 1397–1410. https://doi.org/10.2353/ajpath.2010.090945.

54. Carey, A.N., Sypek, E.I., Singh, H.D., Kaufman, M.J., and McLaughlin, J.P. (2012). Expression of HIV-Tat protein is associated with learning and memory deficits in the mouse. Behav. Brain Res. *229*, 48–56. https://doi.org/10.1016/j.bbr.2011.12.019.

55. Hahn, Y.K., Podhaizer, E.M., Farris, S.P., Miles, M.F., Hauser, K.F., and Knapp, P.E. (2015). Effects of chronic HIV-1 Tat exposure in the CNS: heightened vulnerability of males versus females to changes in cell numbers, synaptic integrity, and behavior. Brain Struct. Funct. *220*, 605–623. https://doi.org/10.1007/s00429-013-0676-6.

56. Paris, J.J., Singh, H.D., Ganno, M.L., Jackson, P., and McLaughlin, J.P. (2014). Anxiety-like behavior of mice produced by conditional central expression of the HIV-1 regulatory protein. Tat. Psychopharmacology (Berl) *231*, 2349–2360. https://doi.org/10.1007/s00213-013-3385-1.

57. Paris, J.J., Fenwick, J., and McLaughlin, J.P. (2014). Progesterone protects normative anxiety-like responding among ovariectomized female mice that conditionally express the HIV-1 regulatory protein, Tat, in the CNS. Horm. Beyond Behav. *65*, 445–453. https://doi.org/10.1016/j.yhbeh.2014.04.001.

58. Kesby, J.P., Markou, A., and Semenova, S. (2016). The effects of HIV-1 regulatory TAT protein expression on brain reward function, response to psychostimulants and delay-dependent memory in mice. Neuropharmacology *109*, 205–215. https://doi.org/10.1016/j.neuropharm.2016.06.011.

59. Hahn, Y.K., Paris, J.J., Lichtman, A.H., Hauser, K.F., Sim-Selley, L.J., Selley, D.E., and Knapp, P.E. (2016). Central HIV-1 Tat exposure elevates anxiety and fear conditioned responses of male mice concurrent with altered mu-opioid receptor-mediated G-protein activation and beta-arrestin 2 activity in the forebrain. Neurobiol. Dis. *92*, 124–136. https://doi.org/10.1016/j.nbd.2016.01.014.

60. Yadav-Samudrala, B.J., Dodson, H., Ramineni, S., Kim, E., Poklis, J.L., Lu, D., Ignatowska-Jankowska, B.M., Lichtman, A.H., and Fitting, S. (2024). Cannabinoid receptor 1 positive allosteric modulator ZCZ011 shows differential effects on behavior and the endocannabinoid system in HIV-1 Tat transgenic female and male mice. PLoS One *19*, e0305868. https://doi.org/10.1371/journal.pone.0305868.

61. Yadav-Samudrala, B.J., Gorman, B.L., Barmada, K.M., Ravula, H.P., Huguely, C.J., Wallace, E.D., Peace, M.R., Poklis, J.L., Jiang, W., and Fitting, S. (2024). Effects of acute cannabidiol on behavior and the endocannabinoid system in HIV-1 Tat transgenic female and male mice. Front. Neurosci. *18*, 1358555. https://doi.org/10.3389/fnins.2024.1358555.

62. Yadav-Samudrala, B.J., Gorman, B.L., Dodson, H., Ramineni, S., Wallace, E.D., Peace, M.R., Poklis, J.L., Jiang, W., and Fitting, S. (2024). Effects of acute Delta(9)-tetrahydrocannabinol on behavior and the endocannabinoid system in HIV-1 Tat transgenic female and male mice. Brain Res. *1822*, 148638. https://doi.org/10.1016/j.brainres.2023.148638.

63. Xiang, J.Z., and Brown, M.W. (2004). Neuronal responses related to long-term recognition memory processes in prefrontal cortex. Neuron *42*, 817–829. https://doi.org/10.1016/j.neuron.2004.05.013.

64. Meunier, M., Bachevalier, J., and Mishkin, M. (1997). Effects of orbital frontal and anterior cingulate lesions on object and spatial memory in rhesus monkeys. Neuropsychologia *35*, 999–1015. https://doi.org/10.1016/s0028-3932(97)00027-4.

65. Kolb, B., Buhrmann, K., McDonald, R., and Sutherland, R.J. (1994). Dissociation of the medial prefrontal, posterior parietal, and posterior temporal cortex for spatial navigation and recognition memory in the rat. Cerebr. Cortex *4*, 664–680. https://doi.org/10.1093/cercor/4.6.664.

66. Chiba, A.A., Kesner, R.P., and Gibson, C.J. (1997). Memory for temporal order of new and familiar spatial location sequences: role of the medial prefrontal cortex. Learn. Mem. *4*, 311–317. https://doi.org/10.1101/lm.4.4.311.

67. Mitchell, J.B., and Laiacona, J. (1998). The medial frontal cortex and temporal memory: tests using spontaneous exploratory behaviour in the rat. Behav. Brain Res. *97*, 107–113. https://doi.org/10.1016/s0166-4328(98)00032-1.

68. Torres-Flores, M., and Peña-Ortega, F. (2022). Amyloid Beta Alters Prefrontal-dependent Functions Along with its Excitability and Synaptic Plasticity in Male Rats. Neuroscience *498*, 260–279. https://doi.org/10.1016/j.neuroscience.2022.07.006.

69. Thiruvady, D.R., Georgiou-Karistianis, N., Egan, G.F., Ray, S., Sritharan, A., Farrow, M., Churchyard, A., Chua, P., Bradshaw, J.L., Brawn, T.L., and Cunnington, R. (2007). Functional connectivity of the prefrontal cortex in Huntington's disease. J. Neurol. Neurosurg. Psychiatry *78*, 127–133. https://doi.org/10.1136/jnnp.2006.098368.

70. Narayanan, N.S., Rodnitzky, R.L., and Uc, E.Y. (2013). Prefrontal dopamine signaling and cognitive symptoms of Parkinson's disease. Rev. Neurosci. *24*, 267–278. https://doi.org/10.1515/revneuro-2013-0004.

71. Pervolaraki, E., Hall, S.P., Foresteire, D., Saito, T., Saido, T.C., Whittington, M.A., Lever, C., and Dachtler, J. (2019). Insoluble Abeta overexpression in an App knock-in mouse model alters microstructure and gamma oscillations in the prefrontal cortex, affecting anxiety-related behaviours. Dis. Model. Mech. *12*, dmm040550. https://doi.org/10.1242/dmm.040550.

72. Lok, K., Zhao, H., Shen, H., Wang, Z., Gao, X., Zhao, W., and Yin, M. (2013). Characterization of the APP/PS1 mouse model of Alzheimer's disease in senescence accelerated background. Neurosci. Lett. *557*, 84–89. https://doi.org/10.1016/j.neulet.2013.10.051.

73. Gu, Z., Zhong, P., and Yan, Z. (2003). Activation of muscarinic receptors inhibits beta-amyloid peptide-induced signaling in cortical slices. J. Biol. Chem. *278*, 17546–17556. https://doi.org/10.1074/jbc.M209892200.

74. Liu, P., Jing, Y., Collie, N.D., Campbell, S.A., and Zhang, H. (2011). Pre-aggregated Abeta(25-35) alters arginine metabolism in the rat hippocampus and prefrontal cortex. Neuroscience *193*, 269–282. https://doi.org/10.1016/j.neuroscience.2011.07.054.

75. Proulx, É., Fraser, P., McLaurin, J., and Lambe, E.K. (2015). Impaired Cholinergic Excitation of Prefrontal Attention Circuitry in the TgCRND8 Model of Alzheimer's Disease. J. Neurosci. *35*, 12779–12791. https://doi.org/10.1523/JNEUROSCI.4501-14.2015.

76. Zhuo, J.M., Prakasam, A., Murray, M.E., Zhang, H.Y., Baxter, M.G., Sambamurti, K., and Nicolle, M.M. (2008). An increase in Abeta42 in the prefrontal cortex is associated with a reversal-learning impairment in Alzheimer's disease model Tg2576 APPsw mice. Curr. Alzheimer Res. *5*, 385–391. https://doi.org/10.2174/156720508785132280.

77. Zhuo, J.M., Prescott, S.L., Murray, M.E., Zhang, H.Y., Baxter, M.G., and Nicolle, M.M. (2007). Early discrimination reversal learning impairment and preserved spatial learning in a longitudinal study of Tg2576 APPsw mice. Neurobiol. Aging *28*, 1248–1257. https://doi.org/10.1016/j.neurobiolaging.2006.05.034.

78. Lawrence, A.D., Sahakian, B.J., and Robbins, T.W. (1998). Cognitive functions and corticostriatal circuits: insights from Huntington's disease. Trends Cognit. Sci. *2*, 379–388. https://doi.org/10.1016/s1364-6613(98)01231-5.

79. Lange, K.W., Robbins, T.W., Marsden, C.D., James, M., Owen, A.M., and Paul, G.M. (1992). L-dopa withdrawal in Parkinson's disease selectively impairs cognitive performance in tests sensitive to frontal lobe dysfunction. Psychopharmacology (Berl) *107*, 394–404. https://doi.org/10.1007/BF02245167.

80. Dubois, B., and Pillon, B. (1995). Do cognitive changes of Parkinson's disease result from dopamine depletion? J. Neural. Transm. Suppl. *45*, 27–34.

81. Dubois, B., and Pillon, B. (1997). Cognitive deficits in Parkinson's disease. J. Neurol. *244*, 2–8. https://doi.org/10.1007/pl00007725.

82. Schouten, J., Cinque, P., Gisslen, M., Reiss, P., and Portegies, P. (2011). HIV-1 infection and cognitive impairment in the cART era: a review. AIDS *25*, 561–575. https://doi.org/10.1097/QAD.0b013e3283437f9a.

83. Liu, Y., Jones, M., Hingtgen, C.M., Bu, G., Laribee, N., Tanzi, R.E., Moir, R.D., Nath, A., and He, J.J. (2000). Uptake of HIV-1 tat protein mediated by low-density lipoprotein receptor-related protein disrupts the neuronal metabolic balance of the receptor ligands. Nat. Med. *6*, 1380–1387. https://doi.org/10.1038/82199.

84. Piller, S.C., Jans, P., Gage, P.W., and Jans, D.A. (1998). Extracellular HIV-1 virus protein R causes a large inward current and cell death in cultured hippocampal neurons: implications for AIDS pathology. Proc. Natl. Acad. Sci. USA *95*, 4595–4600. https://doi.org/10.1073/pnas.95.8.4595.

85. King, J.E., Eugenin, E.A., Buckner, C.M., and Berman, J.W. (2006). HIV tat and neurotoxicity. Microb. Infect. *8*, 1347–1357. https://doi.org/10.1016/j.micinf.2005.11.014.

86. McLaurin, K.A., Harris, M., Madormo, V., Harrod, S.B., Mactutus, C.F., and Booze, R.M. (2021). HIV-Associated Apathy/Depression and Neurocognitive Impairments Reflect Persistent Dopamine Deficits. Cells *10*, 2158. https://doi.org/10.3390/cells10082158.

87. McLaurin, K.A., Li, H., Booze, R.M., and Mactutus, C.F. (2019). Disruption of Timing: NeuroHIV Progression in the Post-cART Era. Sci. Rep. *9*, 827. https://doi.org/10.1038/s41598-018-36822-1.

88. Chen, T.W., Wardill, T.J., Sun, Y., Pulver, S.R., Renninger, S.L., Baohan, A., Schreiter, E.R., Kerr, R.A., Orger, M.B., Jayaraman, V., et al. (2013). Ultrasensitive fluorescent proteins for imaging neuronal activity. Nature *499*, 295–300. https://doi.org/10.1038/nature12354.

89. Barker, G.R.I., Bird, F., Alexander, V., and Warburton, E.C. (2007). Recognition memory for objects, place, and temporal order: a disconnection analysis of the role of the medial prefrontal cortex and perirhinal cortex. J. Neurosci. *27*, 2948–2957. https://doi.org/10.1523/JNEUROSCI.5289-06.2007.

90. Brown, M.W., and Aggleton, J.P. (2001). Recognition memory: what are the roles of the perirhinal cortex and hippocampus? Nat. Rev. Neurosci. *2*, 51–61. https://doi.org/10.1038/35049064.

91. Brown, M.W., Wilson, F.A., and Riches, I.P. (1987). Neuronal evidence that inferomedial temporal cortex is more important than hippocampus in certain processes underlying recognition memory. Brain Res. *409*, 158–162. https://doi.org/10.1016/0006-8993(87)90753-0.

92. Fahy, F.L., Riches, I.P., and Brown, M.W. (1993). Neuronal activity related to visual recognition memory: long-term memory and the encoding of recency and familiarity information in the primate anterior and medial inferior temporal and rhinal cortex. Exp. Brain Res. *96*, 457–472. https://doi.org/10.1007/BF00234113.

93. Gaffan, D., and Murray, E.A. (1992). Monkeys (Macaca fascicularis) with rhinal cortex ablations succeed in object discrimination learning despite 24-hr intertrial intervals and fail at matching to sample despite double sample presentations. Behav. Neurosci. *106*, 30–38. https://doi.org/10.1037//0735-7044.106.1.30.

94. Hannesson, D.K., Howland, J.G., and Phillips, A.G. (2004). Interaction between perirhinal and medial prefrontal cortex is required for temporal order but not recognition memory for objects in rats. J. Neurosci. *24*, 4596–4604. https://doi.org/10.1523/JNEUROSCI.5517-03.2004.

95. Ringo, J.L. (1996). Stimulus specific adaptation in inferior temporal and medial temporal cortex of the monkey. Behav. Brain Res. *76*, 191–197. https://doi.org/10.1016/0166-4328(95)00197-2.

96. Xu, C., Yadav-Samudrala, B.J., Xu, C., Nath, B., Mistry, T., Jiang, W., Niphakis, M.J., Cravatt, B.F., Mukhopadhyay, S., Lichtman, A.H., et al. (2022). Inhibitory Neurotransmission Is Sex-Dependently Affected by Tat Expression in Transgenic Mice and Suppressed by the Fatty Acid Amide Hydrolase Enzyme Inhibitor PF3845 via Cannabinoid Type-1 Receptor Mechanisms. Cells *11*, 857. https://doi.org/10.3390/cells11050857.

97. League, A.F., Gorman, B.L., Hermes, D.J., Johnson, C.T., Jacobs, I.R., Yadav-Samudrala, B.J., Poklis, J.L., Niphakis, M.J., Cravatt, B.F., Lichtman, A.H., et al. (2021). Monoacylglycerol Lipase Inhibitor MJN110 Reduces Neuronal Hyperexcitability, Restores Dendritic Arborization Complexity, and Regulates Reward-Related Behavior in Presence of HIV-1 Tat. Front. Neurol. *12*, 651272. https://doi.org/10.3389/fneur.2021.651272.

98. Hermes, D.J., Yadav-Samudrala, B.J., Xu, C., Paniccia, J.E., Meeker, R.B., Armstrong, M.L., Reisdorph, N., Cravatt, B.F., Mackie, K., Lichtman, A.H., et al. (2021). GPR18 drives FAAH inhibition-induced neuroprotection against HIV-1 Tat-induced neurodegeneration. Exp. Neurol. *341*, 113699. https://doi.org/10.1016/j.expneurol.2021.113699.

99. Hermes, D.J., Xu, C., Poklis, J.L., Niphakis, M.J., Cravatt, B.F., Mackie, K., Lichtman, A.H., Ignatowska-Jankowska, B.M., and Fitting, S. (2018). Neuroprotective effects of fatty acid amide hydrolase catabolic enzyme inhibition in a HIV-1 Tat model of neuroAIDS. Neuropharmacology *141*, 55–65. https://doi.org/10.1016/j.neuropharm.2018.08.013.

100. Jacobs, I.R., Xu, C., Hermes, D.J., League, A.F., Xu, C., Nath, B., Jiang, W., Niphakis, M.J., Cravatt, B.F., Mackie, K., et al. (2019). Inhibitory Control Deficits Associated with Upregulation of CB(1)R in the HIV-1 Tat Transgenic Mouse Model of Hand. J. Neuroimmune Pharmacol. *14*, 661–678. https://doi.org/10.1007/s11481-019-09867-w.

101. Morici, J.F., Bekinschtein, P., and Weisstaub, N.V. (2015). Medial prefrontal cortex role in recognition memory in rodents. Behav. Brain Res. *292*, 241–251. https://doi.org/10.1016/j.bbr.2015.06.030.

102. Marks, W.D., Paris, J.J., Schier, C.J., Denton, M.D., Fitting, S., McQuiston, A.R., Knapp, P.E., and Hauser, K.F. (2016). HIV-1 Tat causes cognitive deficits and selective loss of parvalbumin, somatostatin, and neuronal nitric oxide synthase expressing hippocampal CA1 interneuron subpopulations. J. Neurovirol. *22*, 747–762. https://doi.org/10.1007/s13365-016-0447-2.

103. Qrareya, A.N., Mahdi, F., Kaufman, M.J., Ashpole, N.M., and Paris, J.J. (2021). HIV-1 Tat promotes age-related cognitive, anxiety-like, and antinociceptive impairments in female mice that are moderated by aging and endocrine status. Geroscience *43*, 309–327. https://doi.org/10.1007/s11357-020-00268-z.

104. Ghashghaei, H.T., Hilgetag, C.C., and Barbas, H. (2007). Sequence of information processing for emotions based on the anatomic dialogue between prefrontal cortex and amygdala. Neuroimage *34*, 905–923. https://doi.org/10.1016/j.neuroimage.2006.09.046.

105. Salzman, C.D., and Fusi, S. (2010). Emotion, cognition, and mental state representation in amygdala and prefrontal cortex. Annu. Rev. Neurosci. *33*, 173–202. https://doi.org/10.1146/annurev.neuro.051508.135256.

106. Brandt, C., Zvolensky, M.J., Woods, S.P., Gonzalez, A., Safren, S.A., and O'Cleirigh, C.M. (2017). Anxiety symptoms and disorders among adults living with HIV and AIDS: A critical review and integrative synthesis of the empirical literature. Clin. Psychol. Rev. *51*, 164–184. https://doi.org/10.1016/j.cpr.2016.11.005.

107. Ji, J., Zhang, Y., Ma, Y., Jia, L., Cai, M., Li, Z., Zhang, T., and Guo, C. (2024). People who living with HIV/AIDS also have a high prevalence of anxiety disorders: a systematic review and meta-analysis. Front. Psychiatr. *15*, 1259290. https://doi.org/10.3389/fpsyt.2024.1259290.

108. Kaneko, M., Fu, Y., and Stryker, M.P. (2017). Locomotion Induces Stimulus-Specific Response Enhancement in Adult Visual Cortex. J. Neurosci. *37*, 3532–3543. https://doi.org/10.1523/JNEUROSCI.3760-16.2017.

109. Henschke, J.U., Dylda, E., Katsanevaki, D., Dupuy, N., Currie, S.P., Amvrosiadis, T., Pakan, J.M.P., and Rochefort, N.L. (2020). Reward Association Enhances Stimulus-Specific Representations in Primary Visual Cortex. Curr. Biol. *30*, 1866–1880. https://doi.org/10.1016/j.cub.2020.03.018.

110. Makino, H., and Komiyama, T. (2015). Learning enhances the relative impact of top-down processing in the visual cortex. Nat. Neurosci. *18*, 1116–1122. https://doi.org/10.1038/nn.4061.

111. Miller, J.E.K., Miller, B.R., O'Neil, D.A., and Yuste, R. (2022). An increase in spontaneous activity mediates visual habituation. Cell Rep. *39*, 110751. https://doi.org/10.1016/j.celrep.2022.110751.

112. Chaganti, J.R., Heinecke, A., Gates, T.M., Moffat, K.J., and Brew, B.J. (2017). Functional Connectivity in Virally Suppressed Patients with HIV-Associated Neurocognitive Disorder: A Resting-State Analysis. AJNR. Am. J. Neuroradiol. *38*, 1623–1629. https://doi.org/10.3174/ajnr.A5246.

113. Lew, B.J., McCusker, M.C., O'Neill, J., Bares, S.H., Wilson, T.W., and Doucet, G.E. (2023). Resting state network connectivity alterations in HIV: Parallels with aging. Hum. Brain Mapp. *44*, 4679–4691. https://doi.org/10.1002/hbm.26409.

114. Nguchu, B.A., Zhao, J., Wang, Y., Li, Y., Wei, Y., Uwisengeyimana, J.d.D., Wang, X., Qiu, B., and Li, H. (2020). Atypical Resting-State Functional Connectivity Dynamics Correlate With Early Cognitive Dysfunction in HIV Infection. Front. Neurol. *11*, 606592. https://doi.org/10.3389/fneur.2020.606592.

115. Gabbott, P.L.A., Warner, T.A., Jays, P.R.L., Salway, P., and Busby, S.J. (2005). Prefrontal cortex in the rat: projections to subcortical autonomic, motor, and limbic centers. J. Comp. Neurol. *492*, 145–177. https://doi.org/10.1002/cne.20738.

116. Kim, C.K., Ye, L., Jennings, J.H., Pichamoorthy, N., Tang, D.D., Yoo, A.C.W., Ramakrishnan, C., and Deisseroth, K. (2017). Molecular and Circuit-Dynamical Identification of Top-Down Neural Mechanisms for Restraint of Reward Seeking. Cell *170*, 1013–1027. https://doi.org/10.1016/j.cell.2017.07.020.

117. Murugan, M., Jang, H.J., Park, M., Miller, E.M., Cox, J., Taliaferro, J.P., Parker, N.F., Bhave, V., Hur, H., Liang, Y., et al. (2017). Combined Social and Spatial Coding in a Descending Projection from the Prefrontal Cortex. Cell *171*, 1663–1677. https://doi.org/10.1016/j.cell.2017.11.002.

118. Otis, J.M., Namboodiri, V.M.K., Matan, A.M., Voets, E.S., Mohorn, E.P., Kosyk, O., McHenry, J.A., Robinson, J.E., Resendez, S.L., Rossi, M.A., and Stuber, G.D. (2017). Prefrontal cortex output circuits guide reward seeking through divergent cue encoding. Nature *543*, 103–107. https://doi.org/10.1038/nature21376.

119. Kitamura, T., Ogawa, S.K., Roy, D.S., Okuyama, T., Morrissey, M.D., Smith, L.M., Redondo, R.L., and Tonegawa, S. (2017). Engrams and circuits crucial for systems consolidation of a memory. Science *356*, 73–78. https://doi.org/10.1126/science.aam6808.

120. Lopez, M.R., Wasberg, S.M.H., Gagliardi, C.M., Normandin, M.E., and Muzzio, I.A. (2024). Mystery of the memory engram: History, current knowledge, and unanswered questions. Neurosci. Biobehav. Rev. *159*, 105574. https://doi.org/10.1016/j.neubiorev.2024.105574.

121. Tome, D.F., Zhang, Y., Aida, T., Mosto, O., Lu, Y., Chen, M., Sadeh, S., Roy, D.S., and Clopath, C. (2024). Dynamic and selective engrams emerge with memory consolidation. Nat. Neurosci. *27*, 561–572. https://doi.org/10.1038/s41593-023-01551-w.

122. Hirano, K., Morishita, Y., Minami, M., and Nomura, H. (2022). The impact of pitolisant, an H_3 receptor antagonist/inverse agonist, on perirhinal cortex activity in individual neuron and neuronal population levels. Sci. Rep. *12*, 7015. https://doi.org/10.1038/s41598-022-11032-y.

123. Nass, S.R., Lark, A.R.S., Hahn, Y.K., McLane, V.D., Ihrig, T.M., Contois, L., Napier, T.C., Knapp, P.E., and Hauser, K.F. (2021). HIV-1 Tat and morphine decrease murine inter-male social interactions and associated oxytocin levels in the prefrontal cortex, amygdala, and hypothalamic paraventricular nucleus. Horm. Behav. *133*, 105008. https://doi.org/10.1016/j.yhbeh.2021.105008.

124. Degenetais, E., Thierry, A.M., Glowinski, J., and Gioanni, Y. (2003). Synaptic influence of hippocampus on pyramidal cells of the rat prefrontal cortex: an *in vivo* intracellular recording study. Cerebr. Cortex *13*, 782–792. https://doi.org/10.1093/cercor/13.7.782.

125. Tierney, P.L., Dégenètais, E., Thierry, A.M., Glowinski, J., and Gioanni, Y. (2004). Influence of the hippocampus on interneurons of the rat prefrontal cortex. Eur. J. Neurosci. *20*, 514–524. https://doi.org/10.1111/j.1460-9568.2004.03501.x.

126. Chao, O.Y., Huston, J.P., Li, J.S., Wang, A.L., and de Souza Silva, M.A. (2016). The medial prefrontal cortex-lateral entorhinal cortex circuit is essential for episodic-like memory and associative object-recognition. Hippocampus *26*, 633–645. https://doi.org/10.1002/hipo.22547.

127. Ingiosi, A.M., Hayworth, C.R., Harvey, D.O., Singletary, K.G., Rempe, M.J., Wisor, J.P., and Frank, M.G. (2020). A Role for Astroglial Calcium in Mammalian Sleep and Sleep Regulation. Curr. Biol. *30*, 4373–4383. https://doi.org/10.1016/j.cub.2020.08.052.

128. Taghdiri, N., Calcagno, D.M., Fu, Z., Huang, K., Kohler, R.H., Weissleder, R., Coleman, T.P., and King, K.R. (2021). Macrophage calcium reporter mice reveal immune cell communication *in vitro* and *in vivo*. Cell Rep. Methods *1*, 100132. https://doi.org/10.1016/j.crmeth.2021.100132.

129. Umpierre, A.D., Bystrom, L.L., Ying, Y., Liu, Y.U., Worrell, G., and Wu, L.J. (2020). Microglial calcium signaling is attuned to neuronal activity in awake mice. Elife *9*, e56502. https://doi.org/10.7554/eLife.56502.

130. Lueptow, L.M. (2017). Novel Object Recognition Test for the Investigation of Learning and Memory in Mice. J. Vis. Exp. *126*, 55718. https://doi.org/10.3791/55718.

131. Antunes, M., and Biala, G. (2012). The novel object recognition memory: neurobiology, test procedure, and its modifications. Cogn. Process. *13*, 93–110. https://doi.org/10.1007/s10339-011-0430-z.

132. Ennaceur, A., and Delacour, J. (1988). A new one-trial test for neurobiological studies of memory in rats. 1: Behavioral data. Behav. Brain Res. *31*, 47–59. https://doi.org/10.1016/0166-4328(88)90157-x.

133. Montaldi, D., Spencer, T.J., Roberts, N., and Mayes, A.R. (2006). The neural system that mediates familiarity memory. Hippocampus *16*, 504–520. https://doi.org/10.1002/hipo.20178.

134. Alfar, H.R., Pariser, D.N., Chanzu, H., Joshi, S., Coenen, D.M., Lykins, J., Prakhya, K.S., Potash, M.J., Chao, W., Kelschenbach, J., et al. (2023). Protocol for optimizing production and quality control of infective EcoHIV virions. STAR Protoc. *4*, 102368. https://doi.org/10.1016/j.xpro.2023.102368.

135. Gu, C.J., Borjabad, A., Hadas, E., Kelschenbach, J., Kim, B.H., Chao, W., Arancio, O., Suh, J., Polsky, B., McMillan, J., et al. (2018). EcoHIV infection of mice establishes latent viral reservoirs in T cells and active viral reservoirs in macrophages that are sufficient for induction of neurocognitive impairment. PLoS Pathog. *14*, e1007061. https://doi.org/10.1371/journal.ppat.1007061.

136. Honeycutt, J.B., Liao, B., Nixon, C.C., Cleary, R.A., Thayer, W.O., Birath, S.L., Swanson, M.D., Sheridan, P., Zakharova, O., Prince, F., et al. (2018). T cells establish and maintain CNS viral infection in HIV-infected humanized mice. J. Clin. Investig. *128*, 2862–2876. https://doi.org/10.1172/JCI98968.

137. Honeycutt, J.B., Wahl, A., Files, J.K., League, A.F., Yadav-Samudrala, B.J., Garcia, J.V., and Fitting, S. (2024). In situ analysis of neuronal injury and neuroinflammation during HIV-1 infection. Retrovirology *21*, 11. https://doi.org/10.1186/s12977-024-00644-z.

138. Santa-Cecilia, F.V., Leite, C.A., Del-Bel, E., and Raisman-Vozari, R. (2019). The Neuroprotective Effect of Doxycycline on Neurodegenerative Diseases. Neurotox. Res. *35*, 981–986. https://doi.org/10.1007/s12640-019-00015-z.

139. Chauhan, A., Turchan, J., Pocernich, C., Bruce-Keller, A., Roth, S., Butterfield, D.A., Major, E.O., and Nath, A. (2003). Intracellular human immunodeficiency virus Tat expression in astrocytes promotes astrocyte survival but induces potent neurotoxicity at distant sites via axonal transport. J. Biol. Chem. *278*, 13512–13519. https://doi.org/10.1074/jbc.M209381200.

140. Friard, O., and Gamba, M. (2016). BORIS: A free, versatile open-source event-logging software for video/audio coding and live observation. Methods Ecol. Evol. *7*, 1325–1330. https://doi.org/10.1111/2041-210x.12584.

141. Yadav-Samudrala, B.J., Ravula, H.P., Barmada, K.M., Dodson, H., Poklis, J.L., Ignatowska-Jankowska, B.M., Lichtman, A.H., Reissner, K.J., and Fitting, S. (2024). Acute Effects of Monoacylglycerol Lipase Inhibitor ABX1431 on Neuronal Hyperexcitability, Nociception, Locomotion, and the Endocannabinoid System in HIV-1 Tat Male Mice. Cannabis Cannabinoid Res. *9*, 1500–1513. https://doi.org/10.1089/can.2023.0247.

142. Giovannucci, A., Friedrich, J., Gunn, P., Kalfon, J., Brown, B.L., Koay, S.A., Taxidis, J., Najafi, F., Gauthier, J.L., Zhou, P., et al. (2019). CaImAn an open source tool for scalable calcium imaging data analysis. Elife *8*, e38173. https://doi.org/10.7554/eLife.38173.

143. Pnevmatikakis, E.A., Soudry, D., Gao, Y., Machado, T.A., Merel, J., Pfau, D., Reardon, T., Mu, Y., Lacefield, C., Yang, W., et al. (2016). Simultaneous Denoising, Deconvolution, and Demixing of Calcium Imaging Data. Neuron *89*, 285–299. https://doi.org/10.1016/j.neuron.2015.11.037.

144. Zhou, P., Resendez, S.L., Rodriguez-Romaguera, J., Jimenez, J.C., Neufeld, S.Q., Giovannucci, A., Friedrich, J., Pnevmatikakis, E.A., Stuber, G.D., Hen, R., et al. (2018). Efficient and accurate extraction of *in vivo* calcium signals from microendoscopic video data. Elife *7*, e28728. https://doi.org/10.7554/eLife.28728.

145. Friedrich, J., Zhou, P., and Paninski, L. (2017). Fast online deconvolution of calcium imaging data. PLoS Comput. Biol. *13*, e1005423. https://doi.org/10.1371/journal.pcbi.1005423.

146. Baylor, D.A., Nunn, B.J., and Schnapf, J.L. (1987). Spectral sensitivity of cones of the monkey Macaca fascicularis. J. Physiol. *390*, 145–160. https://doi.org/10.1113/jphysiol.1987.sp016691.

147. Erlich, J.C., Brunton, B.W., Duan, C.A., Hanks, T.D., and Brody, C.D. (2015). Distinct effects of prefrontal and parietal cortex inactivations on an accumulation of evidence task in the rat. Elife *4*, e05457. https://doi.org/10.7554/eLife.05457.

148. Zolin, A., Cohn, R., Pang, R., Siliciano, A.F., Fairhall, A.L., and Ruta, V. (2021). Context-dependent representations of movement in Drosophila dopaminergic reinforcement pathways. Nat. Neurosci. *24*, 1555–1566. https://doi.org/10.1038/s41593-021-00929-y.

149. Roitman, J.D., and Shadlen, M.N. (2002). Response of neurons in the lateral intraparietal area during a combined visual discrimination reaction time task. J. Neurosci. *22*, 9475–9489. https://doi.org/10.1523/JNEUROSCI.22-21-09475.2002.

STAR★METHODS

KEY RESOURCES TABLE

REAGENT or RESOURCE	SOURCE	IDENTIFIER
Bacterial and virus strains		
pAAV-Syn-GCaMP6f-WPRE-SV40	Chen et al.[88]	RRID: Addgene_100837; Cat#100837-AAV1
Chemicals, peptides, and recombinant proteins		
Isoflurane	Pivetal	Cat#07-894-9579
Medical grade oxygen	Airgas	Cat#OX USP125
Betadine solution	Atlantis Consumer Healthcare	Cat#A1123
Lidocaine and Prilocaine Cream	Padagis	Cat#0574-2042-30
Silicone Adhesive	World Precision Instruments	Cat#KWIK-SIL
C&B Metabond L-Radiopaque Powder	Parkell	Cat#S396
C&B Metabond Quick Base	Parkell	Cat#S398
C&B Metabond Universal Catalyst	Parkell	Cat#S371
Meloxicam 5 mg/mL solution	Pivetal	Cat#07-893-7565
Hoechst 33342	Life Technologies	Cat#H3570
Deposited data		
Mendeley Data	This paper	https://doi.org/10.17632/62z7892yr9.1
Experimental models: Organisms/strains		
Mouse: HIV-1 Tat transgenic	Bruce-Keller et al.[50] Chauhan at al.[139]	In-house breeding
Software and algorithms		
Inscopix Data Acquisition Software (IDAS)	Inscopix	www.inscopix.com/
Inscopix Data Processing Software (IDPS)	Inscopix	www.inscopix.com/
Inscopix Data Exploration, Analysis, and Sharing Platform (IDEAS)	Inscopix	www.inscopix.com/
ANY-maze	Stoelting Co.	www.any-maze.com
BORIS	Friard and Gamba[140]	www.boris.unito.it
Prism	GraphPad	www.graphpad.com
Adobe Illustrator	Adobe	www.adobeillustrator.com
Statistical Package for the Social Sciences (SPSS)	IBM	https://www.ibm.com/
Python	Python	www.python.org
Zen 2018 Blue Edition	Zeiss	www.zeiss.com/zen
Biorender	Biorender	www.biorender.com
Other		
DOX chow (6000 ppm, G)	Inotiv	Cat#TD.09282
Stereotaxic instrument	Koph Instruments	Model 942 Small Animal
Micro syringe pump injector	World Precision Instruments	Cat#UMP3T-1
Warming pad and rectal probe	Kent Scientific	RightTemp Jr.
Micro drill burr (0.5 mm)	Fine Science Tools	Cat#19008-05
Trephine drill bit	Fine Science Tools	Cat#18004-18
Skull screws	Glass and Watch Screws	Cat#JT69900
Microsyringe syringe	World Precision Instruments	NANOFIL
36G beveled needle	World Precision Instruments	NF36BV
Surgifoam: absorbable gelatin sponge	Ethicon Surgical Technologies	Cat#1971
AutoClip kit	Fine Science Tools	Cat#12020-00
ProView™ integrated lens (1 mm × 4 mm)	Inscopix	Cat#100-005619

(*Continued on next page*)

Continued

REAGENT or RESOURCE	SOURCE	IDENTIFIER
ProView™ implant kit	Inscopix	Cat#100-004239
Dummy microscope	Inscopix	Cat#1050-003760
Baseplate cover	Inscopix	Cat#100-002388
nVista 3 system	Inscopix	www.inscopix.com/nvista-system/
Open field chamber	Med Associates	Cat#ENV-307
e3 Vision camera	White Matter	www.white-matter.com/
Tissue-Plus OCT compound	Fisher Scientific	Cat#23-730-571
Superfrost™ Plus Microscopic Slides	Fisher Scientific	Cat#12-550-15
VectaShield	Vector Laboratories	Cat#H-1400
Cryostat	Leica	Cat#CM300
Laser scanning confocal microscope	Zeiss	LSM800

EXPERIMENTAL MODEL AND STUDY PARTICIPANT DETAILS

Mice

HIV-1 Tat transgenic mice developed on a hybrid C57BL/6J background were used.[50,139] Mice were bred at the University of North Carolina at Chapel Hill animal facility and were between 2 and 4 months of age during the time of surgery. Mice were housed in a temperature and humidity-controlled housing facility under a 12 h dark cycle with *ad libitum* access to food and water. A total of 24 mice were used for the behavioral experiments and were allocated to two groups based on their genotype [12(6f) Tat(−) mice and 12(6f) Tat(+) mice]. Out of the 24 mice, 8 male mice [5 Tat(−) and 3 Tat(+) mice] were used for the *in vivo* calcium imaging studies. Only male mice were used for *in vivo* calcium imaging due to their larger size at 2–3 months of age that facilitated surgical procedures. Based on past studies, all animals received doxycycline chow for 2 months.[60,62,97,141] Additionally, to control for any effects of doxycycline itself both Tat(–) and Tat(+) mice were placed on DOX chow. All experiments were approved by the University of North Carolina at Chapel Hill Institutional Animal Care and Use Committees and were conducted in accordance with the National Institute of Health guidelines for the Care and Use of Laboratory Animals.

Ethical approval declaration

All the behavioral experiments, survival surgery, and GCaMP microinjection were performed in accordance with the guidelines established by National Institute of Health guidelines for the Care and Use of Laboratory Animals (NIH Publication No. 85-23) and University of Nort Carolina at Chapel Hill Institutional Animal Care and Use Committees (IACUC Protocol No. 23.056).

METHOD DETAILS

Virus

AAV1 encoding GCaMP6f under control of the synapsin promoter, pAAV-Syn-GCaMP6f-WPRE-SV40, drove expression of the green calcium indicator. The viral was injected at a titer of 7 x 10^{12} genomes/mL.

Stereotaxic surgery and viral injection

Mice were anesthetized with 5% isoflurane initially and transferred to the stereotax and kept under 1-2% isoflurane in oxygen (1-2 L/min). A warming pad and a rectal probe were used to monitor and maintain the body temperature throughout the surgery. The hair over the incision cite was trimmed and the skin was prepped with three alternating scrubs of betadine and isopropanol. All the 4 paws of mice were tested via toe-pinch method to access the depth of anesthesia. A midline incision was made to expose the skull, which was leveled, and the connective tissue was removed using a cotton tip applicator. Using the 0.5-mm burr two holes were drilled for the placement of two skull screws. For craniotomy, the trephine drill bit was attached to the microdrill was moved to the desired x, y coordinates (relative to the bregma) AP: 1.87 and ML: +0.5 and the skull was etched away, and the exposed (Figure 1A) tissue was immediately irrigated with sterile saline. Durotomy was performed to facilitate the virus injection and lens implantation. Using the 27 G needle the dura was pierced and carefully peeled away from the brain. Sterile saline and gel foam was applied to stop the bleeding. AAV1 encoding GCaMP6f under control of the synapsin promoter (pAAV-Syn-GCaMP6f-WPRE-SV40, was a gift from Douglas Kim and GENIE Project, was injected into the prefrontal cortex at coordinates (relative to the bregma) AP: +1.87, ML: +0.5, DV: -2.4 using a 10 μL microinjection syringe driven by a micro syringe pump and a 36G needle. Based on preliminary data, a total of 250 nL of GCaMP was infused at a constant slow rate of 100 nL/min and the syringe was left in place for at least 10 min to maximize diffusion before it was carefully withdrawn.

Lens implant

A ProView™ integrated lens (1 mm x 4 mm) attached to the dummy microscope and secured on the arm of the ProView™ implant kit lowered to the final coordinates (relative to the bregma) AP: +1.87, ML: +0.5, DV: -2.1 at a constant rate of ∼100-200 μM/min. A small amount of Kwik-Sil was applied around the lens within the craniotomy to cover any exposed tissue and a head cap was made from Metabond to cover the skull screws and secure the lens in place. To prevent damage to the lens during the daily activities in the home cage, a baseplate cover was fixed on the baseplate. The incision was closed using autoclip surgical staples. Following completion of the surgery, mice were disengaged from the stereotax and topical lidocaine/prilocaine cream was applied to the incision site and ears to help with the discomfort from the ear bars and mice were transferred in a fresh cage. Additionally, 10 mg/kg meloxicam was subcutaneously administered before the surgery began and once a day for the next 5 days. The animals were allowed to recover for at least 2 weeks and the GCaMP expression was checked after 5-6 weeks.

Behavior

Novel object recognition (NOR) task

Mice were acclimated to the weight of the miniaturized epifluorescence microscope (miniscope) for a few days before the start of the experiment. Additionally, mice were also habituated to the open field chamber to ensure that their behavior during the task is not influenced by stress or anxiety. The task consisted of three phases: habituation, training, and testing. On day one, the mouse was anesthetized using isoflurane and the miniscope was attached to the baseplate of the headcap. The mice were placed in their home cage for at least 30 min to recover from anesthesia and then placed in the open field apparatus for habituation for 5 min. The next day, the training phase began with two identical objects (familiar objects) placed equidistant from the center. The mice with the miniscope attached were allowed to explore both the objects for 10 min and returned to the home cage for 1 h (interval) and the miniscope LED was turned off. For the testing phase, one of the familiar objects was randomly replaced by a new object (novel object). Both the familiar and the novel objects were made out of Legos, were approximately 10 cm in height and differed in color and texture and did not differ in odor and size. The miniscope LED was turned on and the mice were allowed to explore for 10 min. Both the familiar and the novel objects were randomized for each mouse. The miniscope was attached to the mice during the training, interval, and testing phase to avoid changes in focus, LED strength, and field of view (FOV) throughout the experiment. A circle in red ink with a diameter of 10 cm was drawn, and the objects were carefully placed at the center of the circle to standardize their location for the behavioral assessment. Time spent exploring the object was defined as either the mouse having 50% or more of its body within the circle at any given moment or directly interacting with the object by touching it. After the behavior experiments the miniscope was removed and the baseplate cover was placed back, and mice were returned to their home cages and housing facility.

Behavior recording and calcium imaging

The NOR task was recorded using the e3 vision camera and the calcium activity was recorded using the nVista 3 miniscope and the Inscopix Data Acquisition Software. Both behavior and calcium activity were recorded at 20 frames per second (fps) and were synchronized by triggering a TTL pulse from the nVista 3 data acquisition box to the e3 vision camera. To identify the events (time when the mice explored the objects) in the behavioral recording were manually annotated using Behavioral Observation Research Interactive Software (BORIS).

Histology

After completion of the behavioral experiments, mice were deeply anesthetized using isoflurane and transcardially perfused with ice cold phosphate buffered saline (PBS) followed by 4% paraformaldehyde (PFA) solution in PBS. Brains were extracted and stored overnight in 4% PFA solution. Following post-fixation, brains were washed in PBS (3 x 1 h) and were subsequently transferred to a 30% sucrose solution for 48 h. Sagittal sections (30 μm) were cut using cryostat and were in 12-well plates containing PBS. Sections were then mounted on glass microscope slides and coverslipped with antifade mounting medium. Images were taken using a confocal microscope and images were acquired by keeping all the parameters constant for all animals (Figure S1).

Behavior statistical analysis

To determine whether there were statical differences in the object exploration of Tat(–) and Tat(+) mice, we ran a two-way ANOVA with repeated measures using SPSS software. Tukey's post hoc test was used to determine significant differences between interactions. Statistical significance was defined as $p < 0.05$.

As a measure of preference for familiar or novel object, in Figure 5, discrimination index was calculated as:

$$\text{Discrimination index} = \frac{t_{NO} - t_{FO}}{t_{NO} + t_{FO}}$$

Where t_{NO} and t_{FO} are the time spent with novel and familiar objects, respectively during the testing phase of the NOR task.

Calcium recording

End-to-End CNMF-E

All the calcium recording data were analyzed using Inscopix Data Exploration, Analysis, and Sharing Platform (IDEAS), unless otherwise noted.

The IDEAS End-to-End CNMF-E workflow extracts data from calcium imaging movies and consists of various processing steps to identify spatial location and temporal dynamics of neurons in fluorescent 1-photon calcium imaging movie and neural events. Below are the steps used by the end-to-end CNMF-E workflow.

Preprocessing

Preprocessing step cropped the movie to a specified pixel region and downsampled it in space and time. The neuronal data were temporally downsampled to 10 Hz by averaging 2 adjacent frames which results in non-overlapping groups of frames to be averaged. Additionally, the calcium movies were also spatially downsampled by a factor of 2. Spatial downsampling helps blur any minor spatial fluctuations, deficits, and reduces processing time.

Spatial bandpass filter

The low and high spatial frequency components of the calcium movies were removed by spatial bandpass filter. Bandpass filtering was performed on each frame by subtracting a high smoothed version of the frame from a low smoothed version of the frame:

$$M_f^{bandpass} = Gaussian\ Blur\left(M_f, \sigma_{high}\right) - Gaussian\ Blur\left(M_f, \sigma_{low}\right)$$

Where $Gaussian\ Blur\left(M_f, \sigma\right)$ represents the 2D spatial convolution of a Gaussian kernel with σ representing the standard deviation in the X and Y dimensions and M_f representing frame f of movie M.

A default value for $\sigma_{high} = 0.5$ and $\sigma_{low} = 0.005$ was used.

Motion correction

Since the calcium movie recorded were in freely behaving mice, any frame-to-frame motion in the movie was removed by the motion correction algorithm. The algorithm initially defines a translation which minimizes the difference between the transformed frame and the reference frame. A maximum translation of 20 was used as default setting and the algorithm then transform every frame of the calcium movie to generate an output movie. The removal of motion artifacts ensures that the spatial location of the cells correspond to the same location across all frames as compared to the pixels visited by their respective cell body over the period of calcium movie. This confirms that the temporal dynamics were due to the changes in the fluorescent reporter and not the displacement of cells.

Project movie

The project movie algorithm calculates a mean frame from a calcium movie. Each pixel in the image of the calcium movie can be calculated as follows:

$$M_{mean}(x,y) = mean_{t\,=\,t_{from},\ldots,t_{to}}\left[M_t(x,y)\right]$$

Where M_t is frame t of a movie M, $t_{from} = 0$, and $t_{to} = T$ where T is the total number of frames in the movie. The result is generated after the calculation is performed for each pixel in the frame.

ΔF/F

The ΔF/F algorithm normalizes each pixel value in the calcium movie to represent a deviation from the baseline value. First, a baseline frame was computed that represents the minimal activity of each pixel which traditionally was the mean frame. The values in the output movie are unit-less and their scale represents deviation from the baseline image and a value of 0.5 equals to 50% increase from the baseline. Each frame of the output movie was calculated as follows:

$$M'(x,y,t) = \frac{M(x,y,t) - F_{baseline}(x,y)}{F_{baseline}(x,y)}\ \forall\,(x,y,t)$$

where $M(x, y, t)$ is the value at pixel coordinate (x, y) of frame t of the movie, M' is the output movie, and $F_{baseline(x,y)}$ is the value of the baseline frame at pixel coordinate (x, y).

CNMF-E

Constrained non-negative matrix factorization (CNMF) was performed to retrieve the temporal dynamics and spatial location of the neurons in a fluorescent 1-photon calcium imaging movie.[142–144] IDEAS reimplemented the CNMF-E in C++ for using it for the data generated through IDAS. Inscopix CNMF-E utilizes multiple steps which encompass the core functionality and were applied to the calcium movie. The steps in the Inscopix CNMF-E algorithm are as follows:

Cell initialization: Every frame of the calcium movie was first high-pass filtered and a correlation and peak-to-noise (PNR) images were generated. For a correlation image, the pixel value is equal to the average correlation over time of that pixel with the eight neighboring pixels whereas in PNR image, a pixel value was equal to the maximum value over time divided by the estimated noise level. By multiplying the correlation and PNR images, a *search image* was generated. The highest valued pixel was assigned as a seed pixel

which was considered to be a potential cell. Based on the algorithm parameters, a box was constructed around the seed pixel and a basic footprint and trace extraction was performed. Finally, the cell footprint was subtracted from the search image, and the process was repeated until no more seed pixels were found.

Background estimation: After the footprint and traces were obtained, the algorithm estimates the background. A ring model was used in which the background at a pixel was estimated as a linear combination of activity for a ring around the pixel. The diameter was calculated by multiplying the ring size factor (used default of 1.4) to the cell size diameter (an average cell diameter of 7 was used in the present study).

Spatial footprints and temporal traces update: The estimated background was subtracted from the calcium movie, and the footprints were re-fitted using the CNMF approach. The footprints were refined and post-processed by smoothing with a median filter, morphological closing, and thresholding. In addition to fixing the spatial footprints and the background, the traces for each cell were optimized in parallel using deconvolution algorithm.[145] The deconvolution was accomplished by modeling the calcium traces from spikes using a simple exponential model as shown by cell traces in Figure 1B. The spikes have an amplitude which ranges from zero to one and ''true'' spikes usually have value were closer to one.

Cell merging and traces extraction: Cell merging algorithm runs after each iteration of spatial and temporal fitting, where it looks for cells that were spatially close and have high temporal correlation. A default merging threshold of 0.7 was used and all the cells with a temporal correlation above 0.7 were automatically merged. The residual of each trace was calculated to obtain a raw version of the traces.

Merge results from all patches: Results from all the independent patches were combined into a single set of spatial footprints and temporal traces. Duplicate cells due to a patch overlap were removed and cells were kept only if their closest patch center matches the patch in which they were identified. In the present study, a patch size (side length of an individual square patch within the field of view) of 80 pixel and patch overlap allowance of 20 pixel was used.

Spatial footprints and temporal traces scaling: The spatial footprints were vectorized and normalized. The corresponding temporal traces were then scaled and an output temporal trace as DF/noise was generated.

Event detection

The event detection identifies bursts of cell activity in the cell set automatically and extracts calcium events from traces. The events were identified by fast increase (monotonic rise) in amplitude followed by a long decay (exponential decay) back to the baseline of the following form:

$$a(t+\delta) = a(t)\exp\left(-\frac{\delta}{\tau}\right)$$

Where t is time in seconds, δ is a period of time in seconds and τ is the mean lifetime in seconds. Here the mean lifetime and the half-life of a decay, $t_{1/2}$ are related as follows:

$$t_{1/2} = \tau \ln(2)$$

The algorithm was run at a default setting of 0.2 seconds. Additionally, there were several computational stages for each input traces which includes:

Median Absolute Deviation which was an estimate of the amplitude of fluctuation from the baseline was calculated as follows:

$$\textit{Median Absolute Deviation} = \textit{median}_i\left(\left|X_i - \textit{median}_j(X_j)\right|\right)$$

Where i and j take the values $1, 2, \ldots, n_{frames}$.

Next, the derivative of the input temporal traces was computed which indicates the change in the amplitude of the traces over a period of time, which tracks the calcium rise and decay.

Another parameter that the algorithms tracks were the negative values from the first derivative, which were then filtered out as false positives. The potential events were required to satisfy three constraints to be classified as an event which were:

Negative transients: The default parameters were set to *Discard Negative Transients* which automatically discards negative amplitude.

Event threshold: if the rise amplitude was below an event threshold, then the event was not valid.

Rate of decay: after the above two constraints were satisfied, the algorithm then computes the decay amplitude. The decay amplitude was calculated as the difference in amplitude from the peak to the point in time where the calcium activity should have decayed completely. If the decay constant was faster than expected, then the event was not valid.

Calcium imaging QC report

The calcium imaging movies usually generate a large data set and therefore it was essential to verify if the data collected was of good quality in order to proceed with secondary analysis. The IDEAS Calcium Imaging Quality Control Tool allows to visualize statistics of the calcium movies, cell sets, and event sets. Figure S5 shows a sample QC report of a calcium movie. The statistics that were reported in the QC tool include:

Movie trends: A decaying exponential was fit (Figure S5) to the calcium data to determine if there were any signs of photobleaching in the movie which was calculated as follows:

$$y(t) = Ae^{-t/\tau} + C$$

Where A is a scale parameter, τ is the time of decay, C is an offset parameter, and $y(t)$ is the best exponential fit.

Projections and footprint view: A figure was generated that outlines the footprints of extracted cells over an image that was derived from the movie.

Traces and events: A figure indicating cell traces for the selected cells along with events from the cells was generated.

Cell set metrics: The cell set metrices generates various interactive scatter plots. The plot shows measures calculated from the footprints of each cell. The roundness which is the circuity was measured using the following:

$$Circuity = \frac{4\pi \, x \, Area}{perimeter^2}$$

The trace quality plot quantifies the quality of cell traces and cell extraction. The y-axis shows the maximum correlation of each cell trace to every other cell trace and the x-axis shows the skew of each trace.

Next, the trace trend plot, shows if the traces decrease or increase over time. The y-axis shows the Spearman rank correlation of each cell trace vs time whereas the x-axis shows the goodness of fit of a decaying exponential to the cell trace. A large absolute value of the Spearman correlation indicate that the trace is monotonically increasing or decreasing, and a large goodness of fit value indicate exponential decay which were rejected by the algorithm.

Event set metrics: When an event set file was included in the QC report algorithm, two event graphs were generated. First, the event rates and signal to noise ratio (SNR) graph where y-axis was the mean event rate for each cell and the x-axis was the SNR obtained from the events and cell traces for each cell. Finally, a decay constant graph was obtained with y-axis as the standard deviation of decay timescales across all events and the x-axis showing median decay timescales for each cell.

Compare neural activity across states

In the present study the states were defined as familiar object and novel object for all the analysis and were run through IDEAS. *Compare neural activity across states* tool exploration calculates the average modulation during familiar and novel object. The algorithm calculates the modulation of neurons during familiar and novel object exploration and validates by permutation testing followed by measuring significance of the modulation scores to identify if each neuron was up or down modulating during familiar and novel object exploration (Figures 5A, 5B, 5I, and 5J). Additionally, a graph with comparison of familiar and novel object exploration against each other for individual cell was also plotted (Figure S3).

Compare neural circuit correlations across states

The algorithm calculates pairwise correlations between cell traces within a cell set for familiar and novel object separately. The correlations during the familiar and novel object were obtained from the behavioral annotation files. The algorithm eliminates the data that had fewer than 10 frames in the recording during familiar or novel object exploration. However, if more than 10 frames of data were not assigned in either of the states, a ''non-state'' was assigned. For the present study, the effect size was calculated between familiar and novel object. The algorithm generates a correlation heatmap (Figures 3A and 3B) for each states, cumulative distribution frequency and a max cell-cell correlation graphs and calculates the effect size using Cohen's d value.

Peri-event analysis

Peri-event analysis has extensively used in the field of systems neuroscience for the analysis of signals from neurons.[146–149] The peri-event analysis tool estimates how the neural activity vary before and after an event timestamp. The algorithm calculates the changes in neural activity of both, entire population of neurons and individual neuron and then classifies them into up-, down-, and non-modulated sub-populations. The peri-event was calculated as Δ activity by calculating the difference between the post- and pre-event activity followed by comparison to a null distribution generated by circularly permuting the event times relating to the neural time series. The tool uses time series traces for each cell from the cell set file and the timestamps from the events file.

For the current study, a visual window for pre- and post-event was set to -2 and 2 seconds, respectively. The neuronal activity for both familiar and novel object was first z-scored which was performed individually for each neuron and then the Δ activity was then computed at population and single-cell level. The Δ activity was plotted as a heat-map and the population average activity was plotted against the null distribution. A significance threshold (α) was performed by two-tailed t test us used to generate p value ($p = \alpha/2$, each side of distribution). The cells were labeled up-, down-, and non-modulated if the bootstrap probability was less than $\alpha/2$, greater than 1 - $\alpha/2$, and between $\alpha/2$ and 1 - $\alpha/2$, respectively.

Combine and compare correlation data

The correlation data from multiple recordings were combined across the familiar and novel object to evaluate the differences in the maximum cell-cell correlation and in the effect size between the two genotypes in the present study. The algorithm runs in two steps, first, combination where the data form the specified groups were aggregated to create a population of cell. A cumulative distribution

function (CDF) (Figures 3C and 3D) and a maximum pairwise comparison between familiar and novel object was plotted (Figures 3E and 3F). A Kolmogorov-Smirnov test was performed to compare the CDF between the genotypes and a Pearson's correlation was performed to test the maximum pairwise correlation.

The second step was comparison, the effect size was calculated for each data set by dividing the difference between the group means by the standard deviation of the data which gives us Cohen's d value (Figure 3G) for which a two-tailed t test was used to compare the means of Tat(–) and Tat(+) data.

Combine and compare population activity data

The population activity data from various recordings were combined and were statistically compared to evaluate if there were differences in the fraction of up- or down-modulated cells. The algorithm works similar to combine and compare correlation workflow, where the data for the defined groups were first combined and then compared to determine if there were any statistical differences. In the combination step, the aggregated population of cells was computed for both type of object exploration and genotype with their corresponding population mean activity. For Figure 4 the neuronal activity was aggregated for four epochs: *before, start, end, after*. Where *before* represents 2 s before the start of the event, *start* and *end* represents the time when the mice starts and stops exploring the object and *after* was 2 s after the end of the event. A Kolmogrov-Smirnov test was performed to evaluate statistical significance for the CDF (Figures 4I–4L) and two-way ANOVA was performed for the average Z scores (Figures 4M and 4N) and the fraction of active cells (Figures 4O and 4P), Tukey's post hoc test was used to determine significant differences between interactions. Statistical significance was defined as $p < 0.05$.

Combine and compare peri-event analysis data

The peri-event data from multiple groups were combined and statistical comparison was performed. The algorithm starts by aligning the time windows from the input files followed by aggregating the data based on cell population. The neuronal activity at each time point was averaged and the neurons from all recordings were pooled together. When averaging across recordings, the data was first averaged across neurons, yielding a single average trace per recording and then averaged together to obtain the group average (Figures 5C, 5E, 5K, and 5M). A paired t test was performed for the combined peri-event data and an independent t-test was performed to access significance for the average Z scores for the up-, down-modulated cells between the Tat(–) and Tat(+) mice (Figures 5D, 5F, 5L, and 5N).

QUANTIFICATION AND STATISTICAL ANALYSIS

All behavioral and *in vivo* calcium imaging analysis results are reported as mean ± SEM unless otherwise specified. Graphs were generated using GraphPad Prism software, and statistical analyses were performed using SPSS software. Statistical significance between groups is indicated in the figures, with detailed statistical tests and corresponding values provided in the figure captions and the results section. For the discrimination index in the NOR task (Figure 2F), an independent t test was conducted to compare Tat(–) and Tat(+) mice. The cumulative distribution functions (Figures 3C, 3D, and 4I–4L) were analyzed using the Kolmogorov-Smirnov test, while maximum cell-cell correlations (Figures 3E and 3F) were assessed using Pearson's correlation. Effect sizes between genotypes (Figure 3G) were calculated using independent t tests, with Cohen's *d* values reported. A two-way ANOVA was performed to evaluate the mean activity of cells during object exploration (Figure 3H). Z scores for the epoch and modulation data in Figures 4 and 5 were analyzed using independent t tests. A two-way mixed ANOVA, with time as a within-subject factor and genotype as a between-subject factor, was applied to assess the mean activity of modulated neurons (Figure 5). Statistical significance was set at $p < 0.05$ for all analyses. A summary of statistical details is provided in Table S1, and additional information for each experiment is included in the respective figure legends.